ACS APPLIED MATERIALS & INTERFACES

www.acsami.org Research Article

Decomposition of Binary Mixtures of DMC/EC, EMC/EC, and DEC/EC on Potassium Surfaces; GC, XPS, and Calculation

Leonie Wildersinn, Daniel Stottmeister, Fabian Jeschull, Axel Groß, and Andreas Hofmann*

Cite This: https://doi.org/10.1021/acsami.4c17461 Read Online

ACCESS | Metrics & More | Article Recommendations | Supporting Information

ABSTRACT: Potassium-ion batteries (KIBs) have emerged as promising candidates for low-cost, high-energy storage systems, driven by their fast ionic conductivity and high operating voltage. To develop advanced KIBs, the performance is usually evaluated in half-cell tests using highly reactive potassium metal, which often leads to misinterpretation of the results due to degradation processes between metal anode and electrolyte components. Here, we systematically investigated the surface reactivity of potassium metal, which is in contact with commonly used solvent combinations, namely, mixtures of ethylene carbonate and linear bis(alkyl)carbonates. Mass spectrometry analysis identified the main electrolyte degradation species, namely, di- and trifunctionalized carbonates, ether-bridged carbonates, and ether-like compounds. Possible reaction pathways for the formation of these products were evaluated by using density functional theory calculations (DFT). X-ray photoelectron spectroscopy showed that potassium metal favors the formation of electrode degradation species, leading to an inorganic rich solid electrolyte interphase composed of K_2CO_3, KOH, and R−OK species. Additionally, we were able to show how the potassium metal itself forms an initial surface layer containing KOH and K_2CO_3. This study highlights the complexity of KIB measurements and clearly reveals the challenges of interpreting half-cell tests.

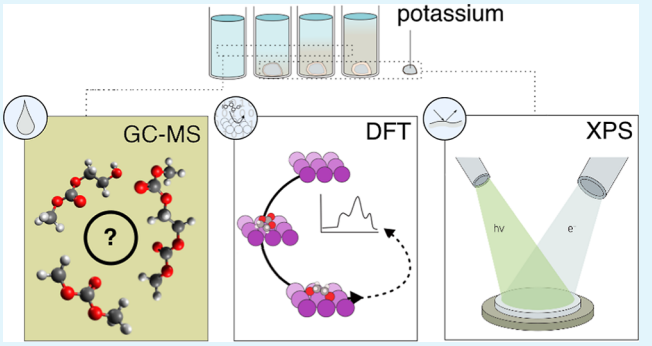

KEYWORDS: *K metal reactivity, GCMS, DFT calculations, XPS, degradation mechanisms*

1. INTRODUCTION

Potassium-ion batteries (KIBs) are emerging as an attractive alternative to lithium-ion batteries (LIBs) offering voltages nearing 4 V, commendable positive and negative electrode capacities, but currently still suffer from short cycle times.[1−3] A key advantage of KIBs is that the cathodes do not rely on scarce or expensive raw materials such as Li, Co and Cu, but instead use inexpensive, abundant elements such as K, Fe, Mn, and C.[2,4] K-ion electrolytes exhibit relatively higher conductivity due to the weaker Lewis acidity of K resulting in smaller radii of solvation and correspondingly lower charge-transfer resistance at the electrode interface because of the smaller desolvation energy.[5] Although significant progress has been made toward developing long cycle life potassium batteries, extensive investigations of electrolytes and their reactivity remain scarce.

When testing electrode materials for applications in KIBs, half cell configurations are usually the first choice to acquire the first electrochemical data. In half cells, the working electrode is cycled against potassium metal to ensure a virtually infinite supply of charge carriers and to avoid limitations by the potassium metal counter electrode (K-CE). This configuration is also relevant for many analytical works, where electrodes are conditioned for further ex situ analysis, such as surface characterization by X-ray photoelectron spectroscopy (XPS).[6,7] However, a number of recent studies pointed out that in the case of KIBs, this can lead to a series of problems that might give rise to misinterpretations and flawed conclusions about the electrode material under investigation.[8−10]

Even at open circuit potentials, there is already a significant amount of surface deposits that originate from degradation reactions at the K-CE.[6,7,11,12] Any surface analysis performed under these conditions thus contains a significant contribution of surface species that are the result of crosstalk and which results in the formation of an unstable solid electrolyte interface (SEI) layer on the potassium anode.[7] In comparison to LIBs, KIBs exhibit a higher organic SEI species content. Since a higher proportion of inorganic components in the SEI is considered favorable for KIBs, it is of great importance to increase the inorganic content through deliberate electrolyte composition. In addition, the understanding of the composi-

Received: October 14, 2024
Revised: January 21, 2025
Accepted: January 22, 2025

tion of the SEI helps to achieve more stable SEI layers in the sense of an artificial SEI. Inorganic compounds are versatile potassium salts such as KF, K_2CO_3, K_2SO_4, and K_2S, while organic compounds are commonly polyesters (RO−COOK) and polyethers (RO−K). Experiments have shown that in the case of KIBs, cycling appears more stable with a SEI rich in inorganic compounds.[8,11,12] Decomposition reactions in the electrolyte play an even greater role in electrochemical experiments that permanently generate new active surfaces (e.g., plating-stripping tests). Indeed, our group has reported that the electrolyte reactivity at the K surface forms electrolyte degradation products that migrate to the working electrode where they are deposited.[6] This crosstalk phenomenon is nearly absent in the graphite-Li systems. This indicates that K-ion chemistries present more severe challenges to the electrolyte and interphase due to more dynamic changes in their electrode structure.[6]

Gas chromatography−mass spectrometry (MS) (GCMS) measurements showed the formation of dicarbonates from the reaction of ethylene carbonate (EC) and a linear carbonate [e.g., dimethyl carbonate (DMC), ethyl methyl carbonate (EMC), or diethyl carbonate (DEC)] in the presence of potassium metal.[7,8] The concentration of dicarbonates in the bulk solution (or electrolyte) depends strongly on the linear carbonate used, namely, DMC or DEC. By extension, this finding was also associated with faster degradation of graphite electrodes in EC/DMC than in EC/DEC mixtures. Moreover, in the case of the commonly used Prussian white $K_2Fe[Fe(CN)_6]$ (KFF), these soluble degradation compounds where also associated with an internal self-discharge caused by reactions at the KFF electrode interface. Hosaka et al. recently demonstrated that this process can be mitigated by the addition of electrolyte additives, specifically 1,3,2-dioxathiolane 2,2-dioxide (DTD).[13−17] The role of DTD in this case is to passivate the potassium metal and curtail the formation of soluble products. However, the authors also reported compatibility issues between the additive and graphite electrodes, rendering DTD as a not a universal solution. Often electrolytes are investigated after exposure to cell potential in order to evaluate decomposition reactions. However, this might trigger reactions through redox processes that differ from those of pure metal−electrolyte interactions.

In a recent study by Pasta and co-workers, it was further shown that the quality of the potassium metal and the preparation from an ingot to a foil has a profound impact on the surface species found by XPS and even the open circuit potential.[9] It was also suggested to pretreat potassium metal while cutting and shaping in electrolyte solutions to receive more repeatable K-CE foils and to achieve an overall better passivation for electrochemical testing.[9] This raises concerns about the repeatability of cell tests in the KIB system, as a reproducible preparation is next to impossible to achieve across different laboratories. Therefore, it is paramount to be aware of the limitations, side reactions, and interferences of half cell experiments that employ K-CEs. This requires a detailed understanding of the formation of the soluble shuttling species at the potassium metal interface and a holistic analytical approach to capture degradation products in the solid and liquid phase.

A well-established tool for the investigation of chemical reactions on the atomistic level is density functional theory (DFT), which can be utilized to gain insights into the surface reactions present in potassium systems. DFT calculations for potassium systems are generally more computationally demanding than calculations for lithium or sodium systems due to the larger number of electrons that have to be taken into account for potassium. This is perhaps one of the reasons for the comparatively low volume of computational studies for potassium (metal) batteries, with the existing literature focusing primarily on solvation effects of the electrolyte with respect to the potassium ion.[18,19] Previous studies have shown that while the degradation reactions of carbonate-based electrolytes on the metal surface show similarities between Li, Na, and K, there are nonetheless important differences that need to be understood.[20] The potassium metal surface with its high reactivity and universal importance for both potassium ion batteries and potassium metal batteries is therefore also of particular interest for DFT studies and molecular dynamics simulations.

Therefore, we combined herein the capabilities of GCMS and XPS as highly sensitive analytical tools with ab initio DFT calculations in order to identify and characterize degradation compounds in the bulk solvent phase and the solid phase at the potassium metal surface and to explore their reaction pathways. In order to simplify the system as much as possible, in the calculations, just the solvent mixtures based on EC and a linear carbonate (DMC, EMC, and DEC) that were exposed to potassium metal foil were considered, i.e., the degradation reactions studied herein do not include interactions with a conducting salt, nor do they involve electrochemical processes. Still the computational findings are relevant for understanding the basic degradation mechanisms. Our results demonstrate in detail the rich chemistry that evolves in mixtures of carbonate solvents in contact with potassium metal. Some of these compounds were previously suspected to form only in the presence of the PF_6^- -anion, but could be also observed in the absence of any conducting salt. To the best of our knowledge, the ab initio DFT calculations in this study are one of the first examples of atomistic DFT studies on processes at the potassium metal interface and greatly support the discussion of possible reaction pathways. Charge analysis of the DFT results was further used in the analysis of the photoemission spectra. Differences in the surface composition upon short exposure of K-metal foils to the solvent mixture agree with reactivity differences among the linear carbonates. Our XPS measurements further highlight the fact that even short exposures to the glovebox atmosphere lead to significant surface layers on potassium metal, with considerable differences in the terms of reactivity toward carbonate solvents.

2. EXPERIMENTAL DETAILS

2.1. Materials. *2.1.1. Sample Handling.* Unless stated differently, materials were used as received and stored under inert gas atmosphere in an Ar-filled glovebox (O_2 < 0.1 ppm, H_2O < 0.1 ppm).

2.1.2. Solvent Preparation. Electrolyte solvent mixtures were prepared from DMC (Gotion, >99.0%, dry), DEC (Gotion, >99.0%, dry), EMC (Merck, >99.0%, dry), and EC (Gotion, >99.0%, dry). Three different solvent mixtures were prepared, each containing 50 vol % EC and 50 vol % of a linear carbonate (DMC, DEC, or EMC).

2.1.3. Sample Aging. The solvent mixtures that had been fabricated as described were placed in a dried glass vial with potassium (prepared as a potassium layer on copper) and then left to stand for a certain time. The vials were not disturbed during storage.

2.2. Gas Chromatography Measurements. GC experiments were performed as described in the literature in detail. Specifically, a Clarus 690 GC device (PerkinElmer Inc., Waltham, USA) was employed, which was equipped with an autosampler, a flame

https://doi.org/10.1021/acsami.4c17461
ACS Appl. Mater. Interfaces XXXX, XXX, XXX−XXX

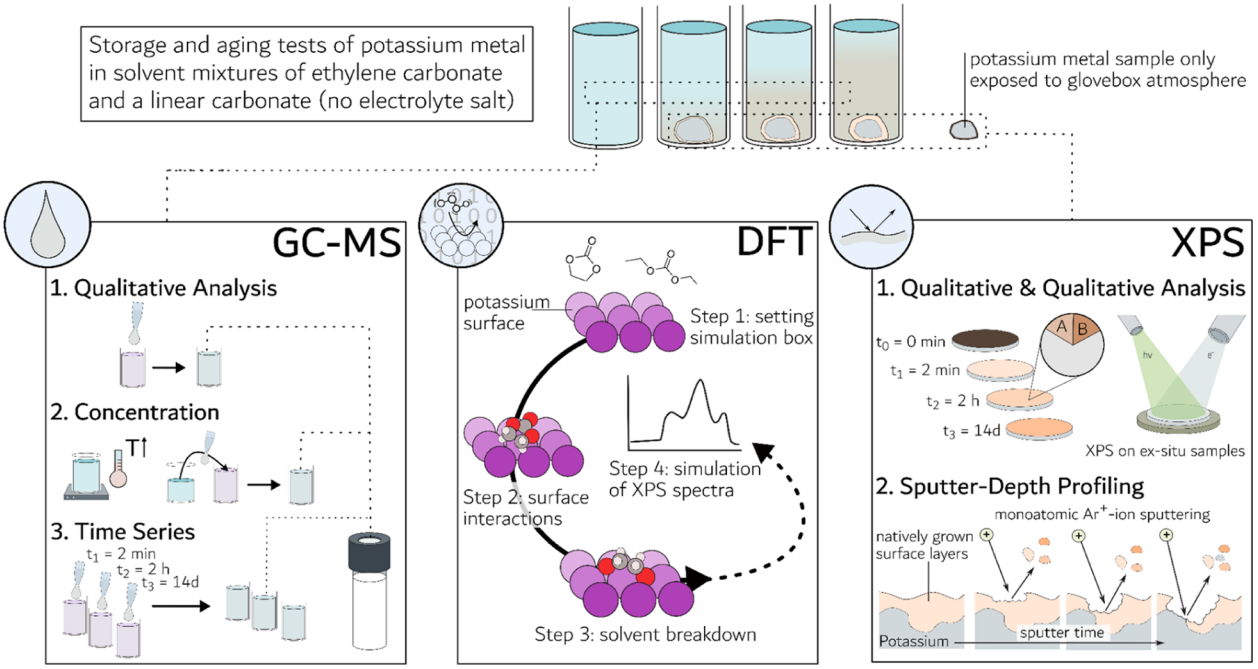

Figure 1. Complementary analytical approach of GCMS and XPS as well as theoretical ab initio DFT calculations combining the results of both individual measurements.

ionization detector (FID), and a MS detector (SQ 8T). After the separation, a gas split was made to be able to use both detectors, the MS and the FID. The Turbomass 6.1.2 and TotalChrom 6.3.4 software packages were utilized for both data acquisition and subsequent analysis. He 6.0 gas (Air Liquide), H_2 gas from a PG + 160 hydrogen generator (Vici DBS) as well as Air (Air Liquide) were used as gases. The GC column utilized was an "Elite 5MS Sil" with a length of 30 m, an interior diameter of 0.25 mm, and a film thickness of 0.5 μm. Injection parameters involved a split flow of 10 mL/min, an inlet temperature of 250 °C, an injection volume of 0.5 μL, an initial pressure of 175 kPa, and a pressure-controlled mode. The oven temperature was maintained at 40 °C. Oven and pressure parameters were set as follows: an initial temperature of 40 °C for 1.5 min, followed by heating at a rate of 20 °C/min up to a final temperature of 320 °C. The initial pressure was maintained at 175 kPa for 2 min and then increased at a rate of 7.8 kPa/min up to a final pressure of 300 kPa. For the MS setup, the filament voltage was set at 70 kV, with ion source temperature of 200 °C and a TransferLine temperature of 200 °C. Postseparation, the gas flow was divided using a SilFlow GC Capillary Column 3-port Splitter to allow signal detection in both the MS and the FID. The MS was operated in scan mode, scanning a range from 33 to 350 u with an event time of 0.3 s and an interscan delay of 0.02 s. All samples, including electrolytes and mixtures, were compared and corrected against pure solvents respectively pure chemicals. Whenever possible, impurities in the electrolyte solvents were identified based on NIST searches [using electron ionization (EI) fragmentation match] and additionally by measuring the pure substance separately.

2.3. XPS Measurements. The XPS measurements were performed using a K-alpha spectrometer (Thermo Fisher Scientific, East Grinstead, UK), applying a microfocused, monochromatized Al Kα X-ray source ($h\nu$ = 1486.6 eV) with 400 μm spot size. In the case of localized surface charging, the binding energy (BE) shifts were minimized using the K-Alpha charge compensation system during analysis, using an electron flood gun with low energy-electrons of 8 eV kinetic energy. Core spectra were recorded with a 0.1 eV step, a constant 50 eV pass energy, and a short time iteration to monitor any possible sample degradation. Reproducibility was confirmed through three measurements of each sample. For intense peaks and/or peaks clearly evidenced by the peak shape, the BE uncertainty was set around ±0.1 eV during curve fitting. In the case of weak peaks and no direct justification by the peak shape, the uncertainty was set to ±0.2 eV. Data acquisition and processing was carried out using the Thermo Avantage software (Version 5.9922, Thermo Scientific). All spectra were referenced to the hydrocarbon C 1s peak (C−C, C−H) at 285.0 eV, while the overall BE scale was controlled by means of the well-known photoelectron peaks of metallic Cu, Ag, and Au, respectively. To provide a clear presentation and more comparable spectra, the intensity was normalized by setting the maximum peak height to 1. Core peaks were utilized depending on the spectral shape, with either a linear or a nonlinear ("smart background") Shirley-type background. For peak fitting, Voigt profiles were used with a 70% Gaussian and 30% Lorentzian contribution, and specific full width at half-maximum constraint ranges were selected to optimize areas and peak positions. The analyzer transmission function, Scofield's sensitivity factors, and effective attenuation lengths for photoelectrons were applied for quantification. Effective attenuation lengths were calculated using the standard TPP-2 M formalism.

2.4. K-Metal Aging Experiments. Samples were prepared in an Ar-filled glovebox (O_2 < 0.1 ppm, H_2O < 0.1 ppm). The K metal (Thermo Fisher, 98% trace metals basis), which was delivered in mineral oil, initially was washed in hexane and then placed and rolled out using a protective PE (polyethylene) sheet in order to reduce sticking to the rolling pin and contamination's on a stainless-steel spacer. The samples were placed in high-density polyethylene vials with 1 mL of the three solvent mixtures mention above and stored in the electrolytes for 2 min, 2 h and 14 days, respectively. After that, the samples were stuck to the XPS sample holder by using Cu-tape. Additionally, 40 μL was extracted from the solvent after the potassium had been stored and analyzed via GC−MS.

2.5. Reference Measurements. The study utilized a range of reference powder samples, as detailed in Table S1 (see the Supporting Information), specifying their supplier names and purity grades. These powders were opened and prepared under an Ar-atmosphere inside a glovebox (O_2 < 0.1 ppm, H_2O < 0.1 ppm). Following this, they were deposited onto an XPS sample holder by pressing them on a sticky Cu tape. Subsequently, the samples were transferred from the Ar-filled glovebox connected to a spectrometer. Notably, no Ar^+-etching was performed in the surface cleaning process to avoid a potential sample degradation. Accordingly, reference substances were also used to prove the compounds identified via mass spectroscopy.

https://doi.org/10.1021/acsami.4c17461
ACS Appl. Mater. Interfaces XXXX, XXX, XXX−XXX

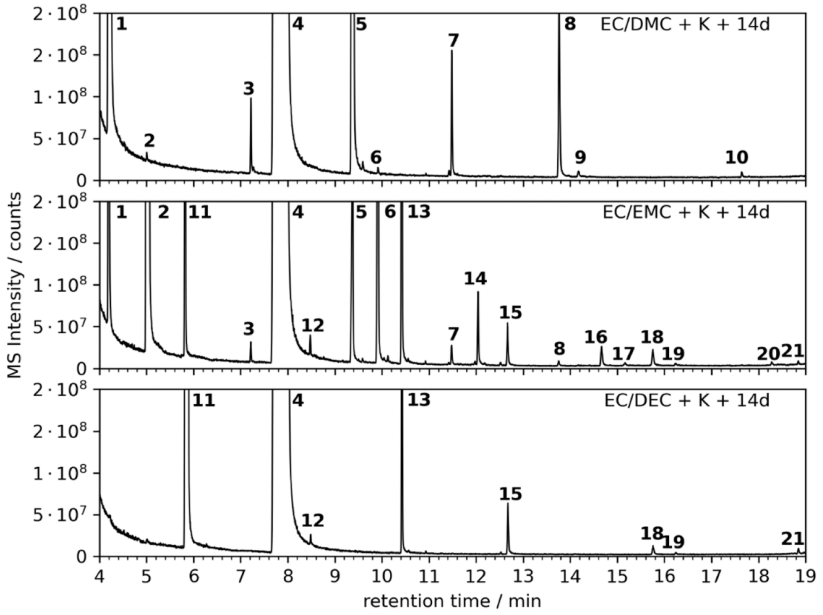

Figure 2. GCMS results of DMC/EC, EMC/EC, and DEC/EC solvent mixtures stored over potassium metal after 14 days. The numbers are assigned in Table 1. The following peaks could not be clarified: **9**, **10**, **17**, **19**, **20**, and **21**.

Table 1. Overview About Solvents and Decomposition Products[d]

abbrev	compound	RI[c]	RI NIST	*m/z* (descending intensity)					no in Figure 1
DMC	dimethyl carbonate	619	620	45	59	90	60	62	1
DEC	diethyl carbonate	782	767	45	91	63	44	75	11
EMC	ethyl methyl carbonate	702	(662)	45	77	59	44	60	2
EC	ethylene carbonate	960	(814)	43	88	44	58	73	4
DMDD	dimethyl 2,5-dioxahexanedioate	1177		59	45	58	91	74	5
DEDD	diethyl 2,5-dioxahexanedioate	1323	(1303)	45	44	91	63	89	13
EMDD	ethyl methyl 2,5-dioxahexanedioate	1251		59	45	77	44	58	6
DMCE	di-(2-methoxycarbonyloxyethyl) ether	1471	(19)	103	59	45	104	70	7
DECE	di-(2-ethoxycarbonyloxyethyl) ether	1613		89	117	45	44	70	15
EMCE	2-ethoxycarbonyloxyethyl-2-methoxycarbonyloxy ethyl ether	1541		103	89	45	117	59	14
DMCC	di-(2-methoxycarbonyloxyethyl) carbonate	1714		59	103	58	45	91	8
DECC	di-(2-ethoxycarbonyloxyethyl) carbonate	1856		44	45	89	117	102	18
EMCC	2-methoxycarbonyloxyethyl-2-ethoxycarbonyloxyethyl carbonate	1782		44	45	59	103	89	16
MEMC	2-methoxyethyl methyl carbonate	926		45	58	59	43	77	3
EEMC	2-Ethoxyethyl methyl carbonate	1004/1011							
MEEC	2-methoxyethyl ethyl carbonate	1004/1011							
EEEC	2-ethoxyethyl ethyl carbonate	1070		72	59	45	89	91	12
MEEMC	2-(2-methoxyethoxy)ethyl methyl carbonate	1211		103	59	58	45	43	
EEEMC	2-(2-ethoxyethoxy)ethyl methyl carbonate	1274/1288							
MEEEC	2-(2-methoxyethoxy)ethyl ethyl carbonate	1274/1288							
EEEEC	2-(2-ethoxyethoxy)ethyl ethyl carbonate	1345		45	89	59	72	73	

[a]Purity of >95% mentioned from the supplier. [b]This is also called "estimated non-polar retention index" in the NIST database. [c]RI, measured with the 5MS capillary column. [d]All individual compounds are measured as pure[a] substances. Provided are GC data including the retention index (RI) as well as mass fragmentation. RI data are related to the onset of the peak. A relation to the peak maximum results in almost equal values (±2). Values in brackets indicate NIST values based on estimation.[b] All compounds are shown in the upcoming sections as chemicals structures.

2.6. Computational Details. All reactions were modeled using ab initio DFT calculations, which are well suited to tackle basic battery-relevant problems employing the plane-wave-based Vienna ab initio simulation package framework.[21,22] The exchange−correlation was calculated using the revised Perdew−Burke−Ernzerhof functional (RPBE) to better account for chemisorption.[23] The electron−core interactions were described via a projector-augmented wave (PAW)-method. Cutoff energy 400/520 eV. A Γ centered 5 × 5 × 1 *k*-point grid was used to calculate the adsorption energies. The electronic self-consistent-field (SCF) was converged up to 10^{-6} eV using the Gaussian smearing scheme with a width of 0.05 eV, with the ionic geometry being converged to energetic differences below 10^{-5} eV. The DFT-D3 van-der-Waals (vdW) correction of Grimme with the zero-dampening method was applied to include dispersion effects during molecular adsorption.[24,25] The surfaces were modeled using a 6 layer slab model with (4 × 4) unit cells topped by a vacuum region with a height in excess of 20 Å. The ab initio molecular dynamics (AIMD) simulations were performed using a Nose thermostat within a canonical ensemble employing a Nose Frequency of 10^{14} Hz at a temperature of 300 K. Charge calculations were performed using the Bader charge analysis method.[26,27]

https://doi.org/10.1021/acsami.4c17461
ACS Appl. Mater. Interfaces XXXX, XXX, XXX−XXX

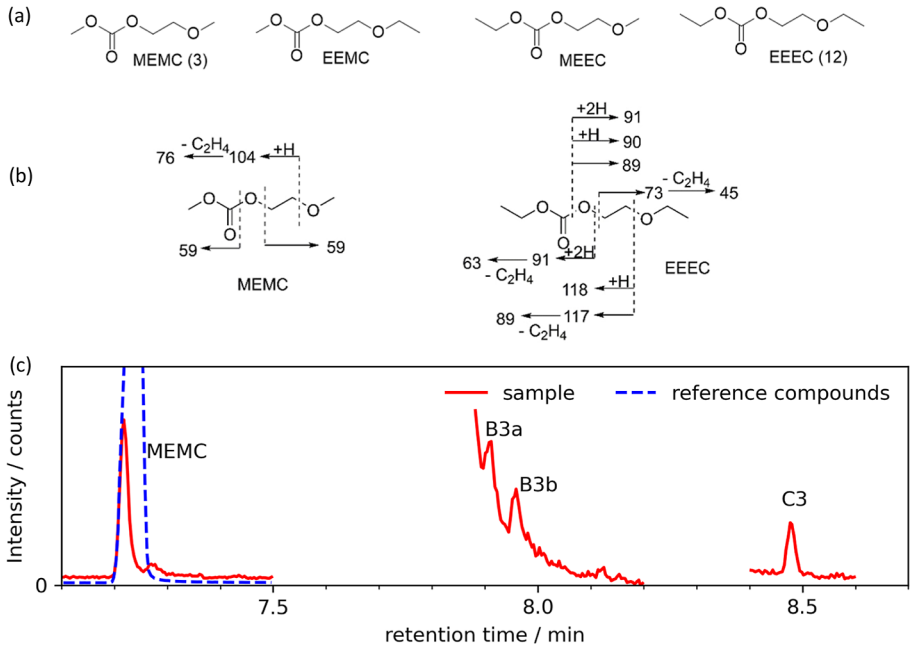

Figure 3. (a) Chemical structures of MEMC (**3**), EEEC (**12**), and their mixed analogue structures (MEEC and EEMC). (b) Mass fragmentation of MEMC and EEEC. (c) Chromatograms of MEMC, B3a, B3b, and C3 in terms of reference substance (blue) and the corresponding compounds formed in the solvent mixtures DMC/EC, EMC/EC, and DEC/EC. The identical retention time (onset) and mass fragmentation (see Figure S13, Supporting Information) proves the formation of the corresponding compound MEMC.

3. RESULTS

In this study, three solvent mixtures were investigated in terms of their reactivity toward potassium metal. The solvent mixtures comprised of 50 vol % EC and 50 vol % of a linear alkyl carbonate, i.e., DMC, EMC, or DEC. For this purpose, a complementary analytical and theoretical approach was chosen, to study the decomposition products as well as the reaction mechanisms (Figure 1).

The first part covers a detailed analysis of the soluble components studied by GCMS (compounds which are liquid or soluble in the solvent mixture and exhibit at least a small vapor pressure), and in the second part, a detailed discussion of the electrode surface from XPS measurements is provided. Building on the experimental results, the reaction mechanisms of solvent molecules at the K-metal interface were studied from a theoretical perspective using ab initio DFT calculations.

3.1. Decomposition Products Formed in the Solvent.

3.1.1. Determination of Decomposition Products by GCMS Analysis. After the solvent mixtures were stored over potassium metal at T = 25 °C, the mixtures were analyzed by GCMS after 14 days (Figure 2). For detailed assignments of the respective compounds observed in Figure 2, pure substances of the suspected compounds were purchased and analyzed under same conditions. Based on the EI mass spectra and retention indices (RI), an unambiguous assignment of the individual signals to certain compounds was possible. A summary of the characteristic analysis data for each compound is given in Table 1.

In addition, the detailed mass spectra are provided in the Supporting Information for each new substance (Figures S1–S6). The mass numbers were obtained on the basis of the EI mass spectra. Nuclear magnetic resonance (NMR) data of the compounds are shown in the Supporting Information (Table S2) in order to facilitate comparability for unknown samples. Unfortunately, the RI values are often missing in the literature, although they would facilitate unambiguous assignment of compounds across different GC instruments. Therefore, the RI values were determined on the basis of the values at peak onset and are based on a comparison with linear alkanes. In addition, Table S3 (Supporting Information) lists all CAS numbers (if available) of the compounds including the full chemical name to ensure unambiguous assignment. The reactants used in the three samples were DMC (**1**), EMC (**2**), DEC (**11**), and EC (**4**). It has been observed that small quantities of DMC and DEC are found in EMC-containing mixtures after storage over potassium metal, as demonstrated in our previous study.[11] The transesterification of EMC to DMC and DEC in the EMC/EC mixture can be clearly seen. To better detect the decomposition products, some of the samples were evacuated. Most of the volatile solvent components DMC, EMC, and DEC were then removed. Chemical formulas of EC, DMC, EMC, and DEC are shown in Figure S7, and the corresponding retention times and mass spectra shown in Figure S8.

The following paragraphs describe the formation of decomposition products that form during the storage of the electrolytes over potassium metal. Such decomposition products are only seen if potassium is present; otherwise, no aging/solvent decomposition was observed. The degradation products are presented according to their retention time hereinafter. As the direct coupling products DMDD, EMDD, and DEDD have already been extensively described in detail in literature as well in an earlier publication before and are thus not discussed again herein.[11,28−33] In short, the results including chemical structures and EI MS spectra are provided in Supporting Information (Section 5, Figures S9–S12).

A group of mixed compounds with ether- and carbonate-terminated sides (mixed oligocarbonate-ethers) was observed with relatively low retention times. Specifically, the monoethers MEMC (**3**), EEEC (**12**), and their mixed-terminal derivatives EEMC and MEEC (Figure 3a). These compounds were

https://doi.org/10.1021/acsami.4c17461
ACS Appl. Mater. Interfaces XXXX, XXX, XXX−XXX

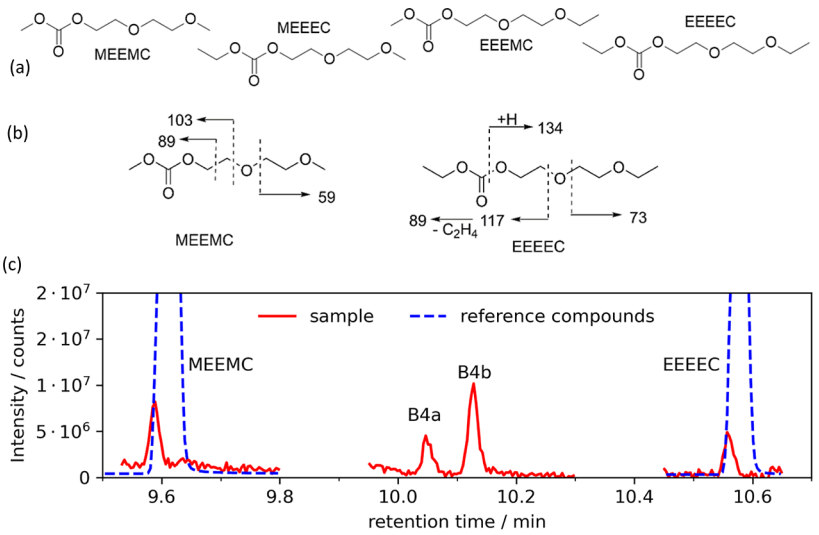

Figure 4. (a) Chemical structures of MEEMC, MEEEC, EEEMC, and EEEEC which formed during the storage over potassium metal in small traces. (b) Mass fragmentation of MEEMC and EEEEC. Typical fragmentation reactions are shown exemplarily. (c) Chromatograms of MEEMC, B4a, B4b, and EEEEC in terms of reference substance (blue) and the corresponding compounds formed in the solvent mixtures DMC/EC, EMC/EC, and DEC/EC. The identical retention time (onset) and mass fragmentation (see Figure S14, Supporting Information) supports the formation of the corresponding compound MEEEC and EEEMC.

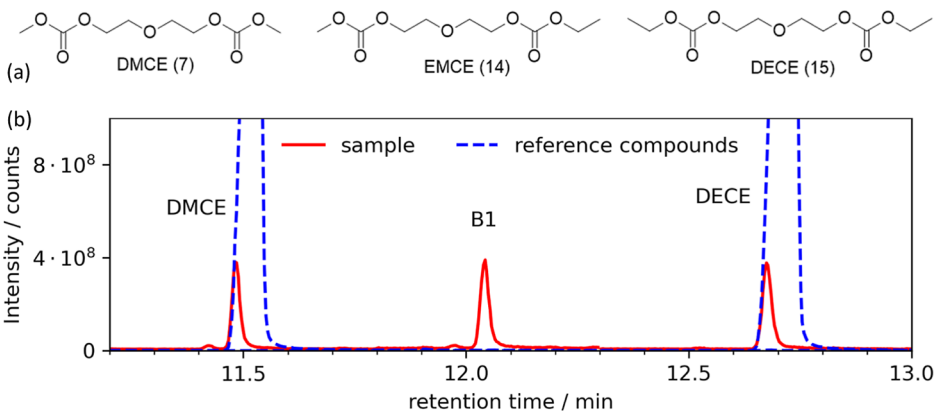

Figure 5. (a) Chemical structures of DMCE (**7**), EMCE (**14**), and DECE (**15**), which formed during the storage over potassium metal. (5b) Chromatograms of DMCE, B1, and DECE in terms of reference substance (blue) and the corresponding compounds formed in the solvent mixtures DMC/EC, EMC/EC, and DEC/EC. The mass fragmentation (see Figure S15) supports the formation of the corresponding compounds DMCE, EMCE, and DECE.

proposed in thermally aged electrolyte samples before, indicating a formation without the need of potential or even metal surfaces.[34] For this series, only the MEMC (**3**) product was commercially available, so the other three products were assigned based on their mass decay and corresponding retention times. This was reasonably close to the corresponding dicarbonate (Δ = 145 RI), tricarbonate (Δ = 142 RI), and ether-bridged carbonate (Δ = 142 RI) compounds with Δ = 144 RI between the MEMC and EEEC (**12**, **C3** in Figure 3a) products.

The mass fragmentation of both products MEMC and EEEC is shown in Figure 3b, and the resulting chromatograms are depicted in Figure 3c. Mass spectral data are provided in the Supporting Information (Figure S13). Typical bulk fragmentations also included the fragments at m/z = 45, 59, 77, and 104 Da (MEMC) and m/z = 45, 59, 63, 89, and 118 Da (EEEC) (Figure 3b). Unfortunately, a clear distinction and assignment of B3a and B3b (Figure 3c) were not possible within this study because both components included fragments of both dialkyl-substituted products. The compounds with mixed methyl/ethyl-terminal groups (EEMC and MEEC) were formed in very small quantities, as indicated by their relative intensities to the main signals from the dimethyl- or diethyl-terminated compounds. The mixed substituted products could only be measured in higher concentrated samples. Since the products were also volatile, the products could not be enriched by evaporation but by column chromatography instead.

In addition to the above monoether moiety, degradation products with diether moieties (also denoted as monoglyme derivatives), termed MEEMC and EEEEC as well as their mixed-terminal derivatives MEEEC and EEEMC (Figure 4), are observed. Such products were proposed before also in case of Li-electrolyte decomposition reactions, respectively, SEI formation.[35] However, these compounds were no longer visible in the chromatogram (Figure 2) directly. They became apparent after the liquid electrolyte was partially evaporated in vacuum and could be measured at a higher concentration (100 μL of the original mixture diluted to 1.5 mL in dichloro-

https://doi.org/10.1021/acsami.4c17461
ACS Appl. Mater. Interfaces XXXX, XXX, XXX−XXX

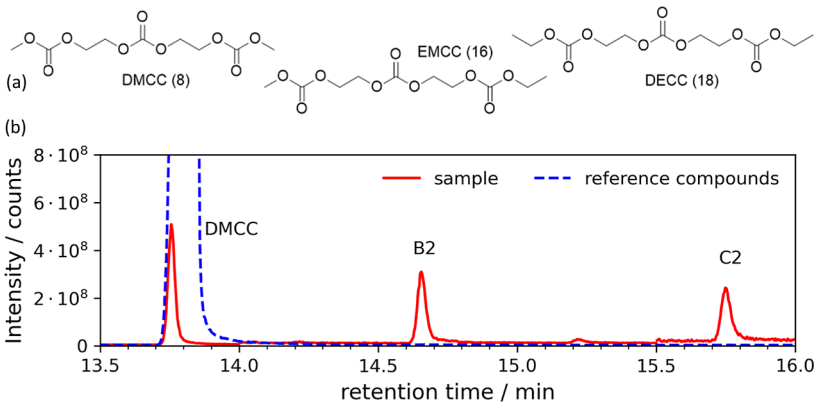

Figure 6. (a) Chemical structures of DMCC (**8**), EMCC (**16**), and DECC (**18**), which formed during the storage over potassium metal. (b) Chromatograms of DMCC, B2, and C2 in terms of reference substance (blue) and the corresponding compounds formed in the solvent mixtures DMC/EC, EMC/EC, and DEC/EC. The identical retention time (onset) and mass fragmentation (see Figure S16) supports the formation of the corresponding compounds DMCC, EMCC, and DECC.

Table 2. Overview of all Liquid Reaction Products Formed During Storage of K for 14 d in Different Solvent Mixtures[a]

K in	dicarbonate-substituted products	ether-bridgedcompounds	trimeric carbonate-substituted products	ether-like products
EMC/EC	**5** (DMDD), **6** (EMDD), **13** (DEDD)	**7** (DMCE), **14** (EMCE), **15** (DECE)	**8** (DMCC), **16** (EMCC), **18** (DECC)	**3** (MEMC), **12** (EEEC), MEEEC, EEEMC
DMC/EC	**5** (DMDD)	**7** (DMCE)	**8** (DMCC)	**3**, MEEMC
DEC/EC	**13** (DEDD)	**15** (DMCE)	**18** (DECC)	**12** (MEMC), EEEEC

[a]The numbers correlate with the numbers given in Figure 1. Names of the compounds are listed in the Supporting Information (Tab. S2).

methane). The compounds have been found to have the very similar retention times compared to the carbonate coupling products DMDD (**5**), EMDD (**6**), and DEDD (**13**). The two products MEEMC and EEEEC were clearly identified as pure compounds based on retention time and mass fragmentation. The mass fragmentation is shown in detail in Figure S14. The m/z values of 59, 89, and 103 for the methyl-substituted product MEEMC and the fragmentation at m/z = 73, 89, and 117 for the ethyl-substituted product EEEEC are particularly noticeable.

Based on the fragmentation patterns (Figure 4b) and the corresponding retention times (Figure 4c) as well as the mass fragmentations (Figure S14) for the mixed products, an assignment can be made. This leads to the conclusion that "B4a" (Figure 4c) can be assigned as EEEMC based on the characteristic mass peaks at m/z = 59 and 103 and the compound "B4b" can be assigned as MEEEC based on the values at m/z = 89 and 117 accordingly.

Another class of compounds found in the samples is the ether-bridged compounds DMCE (**7**), EMCE (**14**), and DECE (**15**, Figure 5). The mass spectra of the individual solvent mixtures are shown in Figures S1−S3. These structures are also proposed in the case of Li-SEI formation by von Holtum et al. for Li-electrolyte mixtures and be observed in case of cycled lithium electrolytes.[30,34]

Both dialkyl compounds DMCE and DECE were measured as pure substances and clearly assigned. Based on the mass spectra, the following characteristic fragments were detected: 59 $[CH_3OCO]^+$, 103 $[MeOC(O)OCH_2CH_2]^+$, 89 $[EtOC(O)O]^+$, 117 $[EtOC(O)OCH_2CH_2]^{+\cdot}$ and 45 $[EtOC(O)-C_2H_4]^+$. The compound labeled "**B1**" in Figure 5b shows fragments of both the dimethyl- and diethyl-terminated compounds (DMCE and DECE) in the mass decay, which suggests based on the mass fragmentation and the retention time the presence of EMCE (**14**), i.e., the ethyl methyl-terminated dialkyl product is present. From the difference in retention indices, it is found that B1 (EMCE) is located between the dialkyl products with ΔRI of 71 ± 1, as discussed before.

Another set of coupling reactions was identified as the trimeric alkyl carbonate-substituted products DMCC (**8**), EMCC (**16**), and DECC (**18**) shown in Figure 6a. The chromatograms are shown in Figure 6b, and mass spectra can be found in the Supporting Information (Figure S16). The finding confirms the formation of such compounds also in case of Li-electrolyte mixtures studied before.[28,33,35] DMCC was confirmed beyond doubt based on the retention time and mass fragmentation of the corresponding synthetic pure compound. The mass spectra of the individual solvent mixtures are shown in Figures S4−S6 (Supporting Information).

In contrast to the ether-bridged compounds, both outer carbonate groups here are also linked by carbonate groups. With regard to fragmentation, very similar patterns are therefore obtained since the C−O bond is preferably cracked. The mass fragments with m/z = 59, 91, 103, 45, 77, 89, 117, and 63, which were already dominant in the dicarbonate products DMDD, EMDD, and DEDD, are found again, based on similar fragmentation. The differences in the RI indices reveal Δ68 and Δ142 m distances from DMCC, respectively. This correlates very well with the shift observed for the corresponding ether compounds (Δ71 and Δ142) and related dicarbonate compounds (Δ73 and Δ146). Hence, the compound denoted as "B2" and "C2" in Figure 6b were assigned to the corresponding ethyl/methyl- and diethyl-terminated compounds, i.e., EMCC (**16**, B2) and DECC (**18**, C2) based on the retention behavior and mass fragmentation.

In Figure 2, other smaller signals can be recognized. However, these could not be fully clarified within the scope

https://doi.org/10.1021/acsami.4c17461
ACS Appl. Mater. Interfaces XXXX, XXX, XXX−XXX

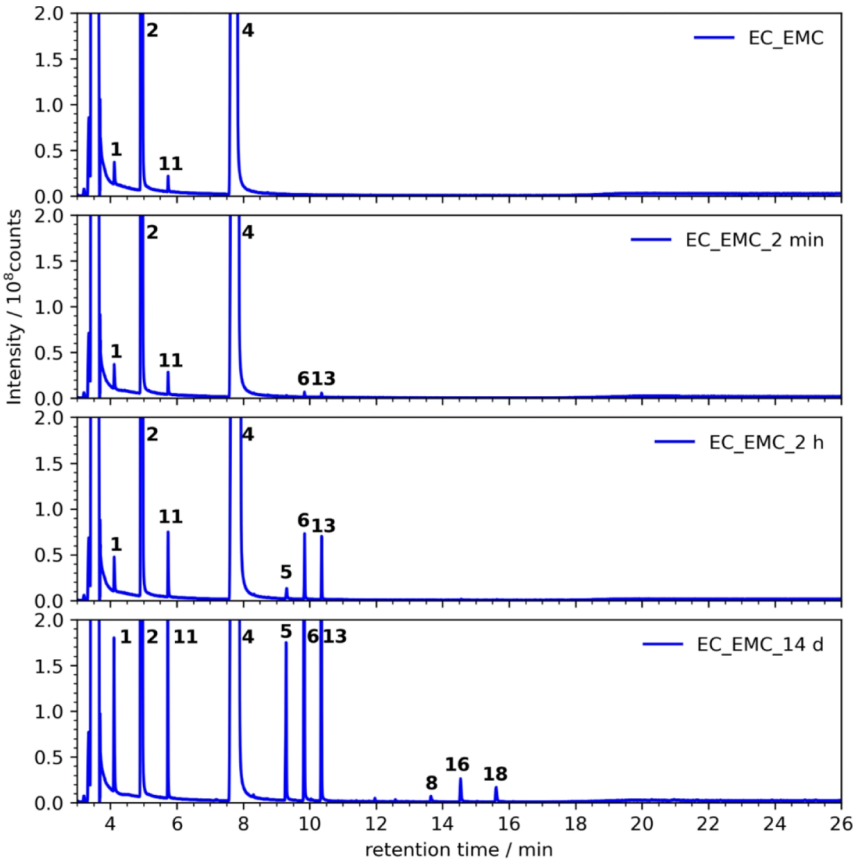

Figure 7. Time-dependent degradation of EC/EMC solvent when K is present. The formation of decomposition products is clearly visible due to the occurrence of peaks at retention times above 8 min. Labeling is in accordance with labels in Figure 1.

of this work. It is assumed on the basis of characteristic mass fragments (m/z = 89, 103, 117, etc., see Figure S17) that coupling products of higher homologues are also present herein, e.g., longer chain mixed oligocarbonate-ethers or pure oligocarbonates.[33] No evidence of the formation of branched monocarbonates, pure ethers, or expanded linear carbonates was observed in this study.[35] The compounds identified in the study, as well as the corresponding reactants, are summarized in Table 2. In order to improve the comparability of the results obtained, it should be pointed out again that it is always useful to include the RI values in order to make a device-independent determination.

3.1.2. Time-Dependent Formation of Decomposition Products in Electrolytes Including Potassium Metal. The study investigated the progression of degradation over time and the compounds that are formed in the initial degradation step. Therefore, the samples were analyzed after 2 min, 2 h, and 14 days. The results for the mixture EC/EMC/K are shown as an example (Figure 7), and the other both mixtures are shown in the Supporting Information (Figures S18 and S19). It is observed that the degradation occurs very quickly and that the first degradation products can be detected after only 2 min. The semiquantitative measurements (the intensity is normalized to the both solvents EC + EMC) show that the dicarbonate products DMDD (**5**), DEDD (**13**), and EMDD (**6**) are already present after 2 min and increase significantly within 2 h, in accordance with our previous results.[11] The known transesterification also leads to an increase in the amounts of DMC (**1**) and DEC (**11**). After 14 days, the concentrations have increased and new decomposition products have formed, in particular the tricarbonates DMCC (**8**), EMCC (**16**), and DECC (**18**). The formation of DMDD from the mixture of EC/DMC is most pronounced within the first two minutes. However, it is apparent that surface reactions occur immediately after the addition of the solvent and that these rapidly lead to a change in the composition of the solvent.

3.1.3. Evaluation of the Role of Glycol in the Formation of Oligomers on the K-Surface Using ab Initio DFT Calculations. Building on the experimental results in the section above, we investigated the energetics of possible reaction mechanisms for forming the linear carbonates detected in the experimental GCMS section.

To ascertain the likelihood of these reactions occurring in our systems, we performed DFT calculations under vacuum conditions and on a K(100) surface. We calculated adsorption energies of possible fragments and also the reaction energies (see eq 1) of the identified reaction pathways according to

$$E_{\text{reaction}} = E_{\text{products}} - \text{E}_{\text{educts}} \quad (1)$$

It is important to note that within this approach, we only take the reaction enthalpy into account. Any entropic or kinetic effects were not explicitly considered in this study.

The adsorption sites for single adsorbates within the chosen (4 × 4) K(100) unit cell were determined by determining the energy minima for a number of possible species. Furthermore, we performed AIMD simulations of DEC and DMC in the presence of EC and PF_6 impinging on K(100) in order to obtain unbiased results of possible reaction products. It has to be noted that these AIMD simulations can only detect possible

https://doi.org/10.1021/acsami.4c17461
ACS Appl. Mater. Interfaces XXXX, XXX, XXX−XXX

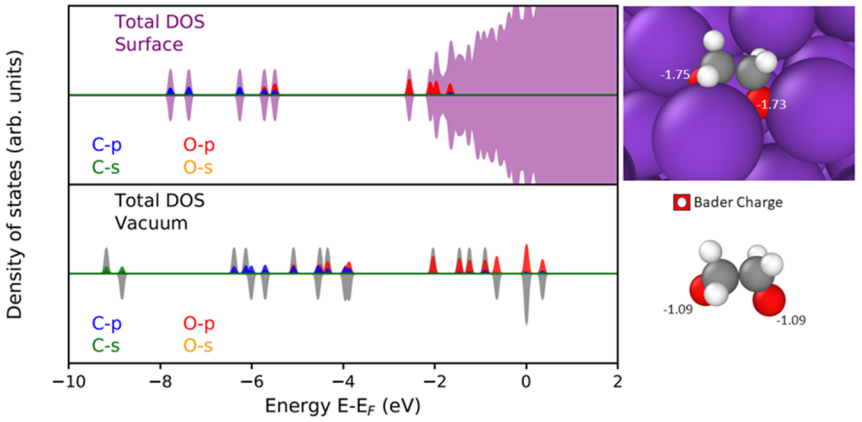

Figure 8. Calculated density of states (DOS) plot and Bader Charges for the investigated $C_2H_4O_2$ fragment on the K(100) surface and in vacuum. The total DOS is depicted in purple for the surface calculation and gray for the vacuum calculation; the partial DOS is shown as spin-up only, and only carbon and oxygen are depicted explicitly. Hydrogen and potassium states are included within the total DOS.

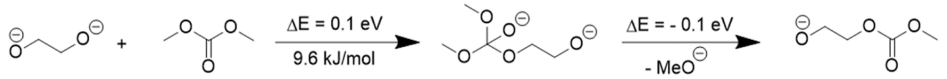

Figure 9. Proposed reaction mechanism for the nucleophilic substitution reaction forming alkoxides on the potassium surface; all reactants are adsorbed on the K-surface. Reaction energies are given in both eV and in kJ/mol.

reaction products that either form spontaneously or only require rather small activation energies.

EC was the common component in all of the tested electrolyte mixtures, which can undergo several decomposition reactions. Among the possible decomposition products of EC, the $[O{-}CH_2{-}CH_2{-}O]^{2-}$ fragment, which has been previously proposed to form on alkali metal surfaces, is of particular interest, due to its possible function as a link between DMC or DEC molecules, resulting in the detected linear carbonates such as DMDD.[19,20] Figure 8 depicts the calculated density of states of the $[O{-}C_2H_4{-}O]^{2-}$ fragment and the oxygen Bader charges on the potassium surface (top panel) and in isolation (vacuum environment, bottom panel), showing a strong partial negative charge on the oxygen atoms on the metal surface. In both cases, the isolated fragment as well as the surface adsorbed fragment, the highest occupied molecular orbital (HOMO) consists of largely oxygen p-states, meaning that any electron donation by the fragment would likely involve the oxygen states. The stabilization of these oxygen p-states near the Fermi level through the potassium surface adsorption can be seen by the downward shift in the energy of the HOMO states. The electronic differences between the isolated and adsorbed species highlight the necessity to include the surface when investigating chemical reactions. Similar plots are provided for other fragments in the Supporting Information in more detail (Figures S20–S27).

Due to the glycolate charges being located at the respective oxygen atoms, we propose a nucleophilic attack of the glycol oxygen on the carbonate group of the target molecule to initiate a nucleophilic substitution reaction, as shown in Figure 9.

This mechanism follows the previously observed selectivity of hard bases to attack the sp^2-hybridized carbon following the hard and soft acids and bases theory.[36] We propose the reaction pathway to follow a condensation reaction with an alkoxide molecule byproduct (MeO), which our XPS measurements readily detected (see below). The calculated density of states and the oxygen Bader charges for the proposed reaction intermediate are depicted in Figure S20 (Supporting Information), where the charge density for intermediate shows an asymmetry for the methoxy-groups both on the surface, as well as in the vacuum environment, hinting toward a relative destabilization of one of the methoxy groups. This break of symmetry is particularly noticeable when the intermediate is compared with the DMC educt, which is depicted in Figure S21 (Supporting Information). Here, both methoxy groups show a nearly symmetrical charge distribution.

Further, a similar tetrahedral intermediate in which carbon is bonded to four oxygen has been shown to exist during the synthesis of polycarbonates.[37] Detected products like DMDD could be formed via this mechanism; however, products like DMCE require a diethylene glycol linking unit (or more generally oligomeric glycolates as bridge between the termal carbonates). Hence, the required chain length exceeds the $[O{-}CH_2{-}CH_2{-}O]^{2-}$ fragment. Based on our simulations, we dismissed the possibility of a chain growth reaction by the addition of a second ethylene glycolate unit through nucleophilic attack (first reaction step in Figure 10). Moreover, in the presence of sp^2-hybridized carbons of the carbonate molecules, a significantly higher preference toward the nucleophilic attack of hard bases like alkoxides ($R{-}O^-$), carboxylates ($R{-}COO^-$), and carbonates ($R{-}O(C{=}O)O^-$)

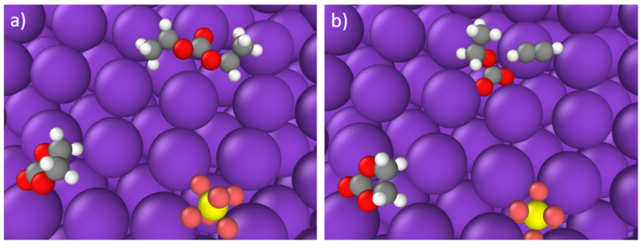

Figure 10. (a) Simulation snapshots of the AIMD simulation of DEC, EC, and PF_6 on a K(100) surface (a) at the start of the simulation, (b) after 5 ps and after the decomposition of DEC.

https://doi.org/10.1021/acsami.4c17461
ACS Appl. Mater. Interfaces XXXX, XXX, XXX−XXX

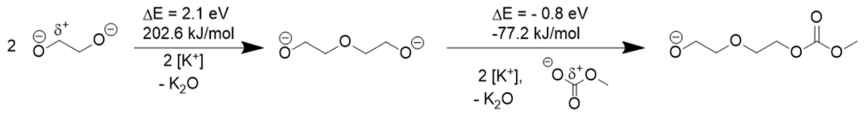

Figure 11. Proposed reaction mechanisms for the condensation reactions forming potassium-oxides on the potassium surface; all reactants are adsorbed on the K-surface.

on DMC is expected. Apart from the nucleophilic substitution reaction, we further investigated an alternative reaction pathway involving the formation of a potassium oxide species on the metal surface. We start once again with the $[O-CH_2-CH_2-O]^{2-}$ fragment; however, in this hypothesized pathway, the nucleophilic attack occurs on a methyl/ethyl carbonate anion formed from DMC/DEC $(RO-C=O)O^-$, R = Me, Et, whose formation was observed in AIMD simulations (see Figure 10).

In the simulation, the DEC molecule decomposes under the release of three hydrogen atoms into the $[CH_3-CH_2-CO_3]^-$ fragment and acetylene (C_2H_2) gas. It must be noted that PF_6 was present within the simulation cell for this specific simulation, which is absent in the experimental setup. However, PF_6 was not involved in the observed formation of ethyl carbonate. Consequently, the formation reaction was deemed possible in the absence of PF_6. Further, the methyl carbonate anion is a known product of the methylation reaction of DMC.[38] The proposed reaction pathway is depicted in Figure 11. We further investigated the possible polymerization reaction of two $[O-CH_2-CH_2-O]^{2-}$ fragments to investigate the formation of longer "connector" molecules, that would allow the formation of products like DMCE (7) (Figure 11).

The adsorption energies of a selection of detected and proposed electrolyte fragments are collected in Table S4.

We find that the proposed nucleophilic substitution reaction nucleophilic attack step is slightly endothermic, requiring 9.6 kJ/mol of energy, while the following condensation reaction was found to be slightly exothermic by almost the exact same amount, resulting in a total reaction energy of −0.01 eV or −0.96 kJ/mol. This low energetic difference between the educt and product would suggest that the reaction is likely to be reversible, which is in agreement with previous works. While we tested this reaction in the presence of a pristine K(100) surface, transesterification reactions of alcohols and DMC are known to occur in the presence of K_2CO_3, which we were able to detect in our measurements.[39] Therefore, it is possible that the formation of products like DMDD is not limited to the potassium surface but could also occur on the formed carbonate surfaces.

The second proposed reaction involving the methylcarbonate anion was found to be exothermic, yielding −77.2 kJ/mol of energy. We therefore conclude that the second proposed reaction could be a viable alternative to the proposed nucleophilic substitution reaction. However, the methylcarbonate anion is known to be rather unstable, typically decomposing into CO_2 and methanolate.[40] This instability would likely result in only a small number of methylcarbonate anions being present at the surface at any given point in time, lowering the chances of any "connector" molecules interacting with said ions before decomposition. Such entropic effects can, however, not be captured within our approach but are likely to decrease the importance of this second reaction path. We further found the polymerization of two $[O-CH_2-CH_2-O]^{2-}$ fragments to be rather unfavorable, requiring 202.6 kJ/mol of energy for the reaction. The direct polymerization of two glycol fragments is therefore deemed unlikely.

We further investigated the possible cleavage of the detected ether connections and proposed the following concerted mechanism (Figure 12).

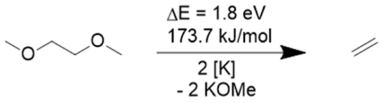

Figure 12. Proposed reaction mechanism via concerted ether bond cleavage on the potassium surface; all reactants are adsorbed on the K-surface.

We find this reaction to be rather energetically demanding (173.7 kJ/mol), making the direct ether cleavage reaction rather unlikely. It is noteworthy, however, that this reaction could easily be entropically driven due to the release of ethene gas, which would likely escape and be unable to participate in a reverse reaction. The formation of linear carbonates similar to the oligomers detected within this work can form via ring opening polymerizations; however, we were unable to detect any ring-species within our experimental analysis, which is why a formation via a ring−opening reaction was deemed to be unlikely.[41] The formation of components such as DMCE (7) remains partially unresolved. The proposed formation of larger linking chains via a direct polymerization was found to be quite endothermic and was therefore deemed to be rather unlikely.[29] The expected linking fragments for DMCE and similar products can be viewed as monomer (ethylene glycol) or oligomer (diethylene glycol or longer) fragments of a potential polyethylene glycol, which can be formed from ethylene oxide.[42] We were unable to detect any ethylene oxide within our experiments, however, leaving the exact origin of the longer connector chains unresolved. Clearly, the reactions considered herein present only a fraction of the K-metal surface. While a holistic description of the chemical space is far beyond the scope of this work, future studies could also build upon earlier experimental studies by Gacchot et al. and Gireaud et al. as a more selective approach.[43,44]

3.1.4. Solid Degradation Products at the Potassium Metal−Electrolyte Interface. Complementary to the soluble degradation products, XPS measurements were carried out to investigate the surface layer composition (and thickness) after 2 min exposure time of potassium metal in the respective solvent mixtures of EC and one of the linear carbonates DMC, EMC, and DEC. The experimental series was expanded to 2 h and 14 days as well; however, there was no significant difference between exposure for 2 min and 2 h, and after 14 days, the surface layer grew too thick (all additional data are provided in the Supporting Information, Figure S28a−c and Table S5).

The XPS analysis is divided into three parts: (1) sputter depth profiling analysis of pristine potassium metal, (2) analysis of solvent-exposed potassium metal surfaces, (3)

https://doi.org/10.1021/acsami.4c17461
ACS Appl. Mater. Interfaces XXXX, XXX, XXX−XXX

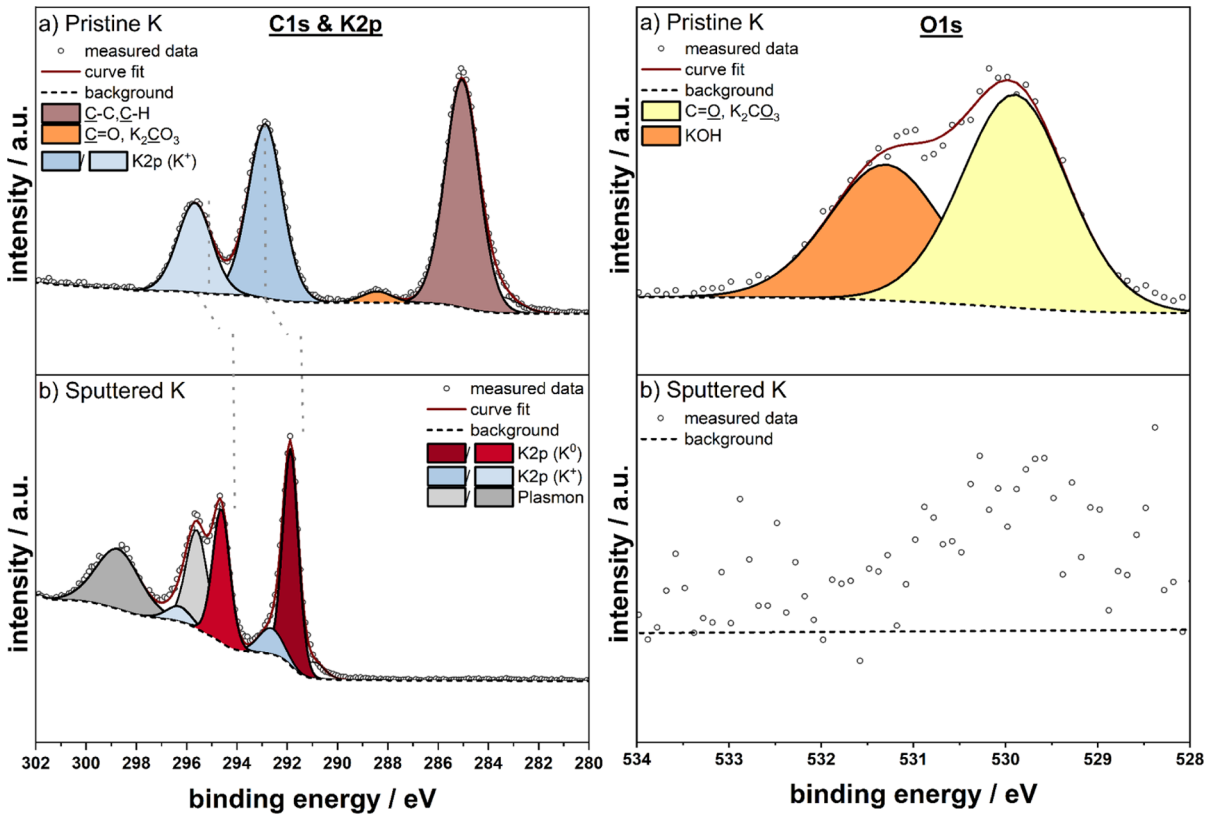

Figure 13. C 1s and K 2p and O 1s spectra of the (a) pristine potassium and (b) sputtered potassium metal. The energy scale is calibrated versus the hydrocarbon peak at 285 eV before sputtering.

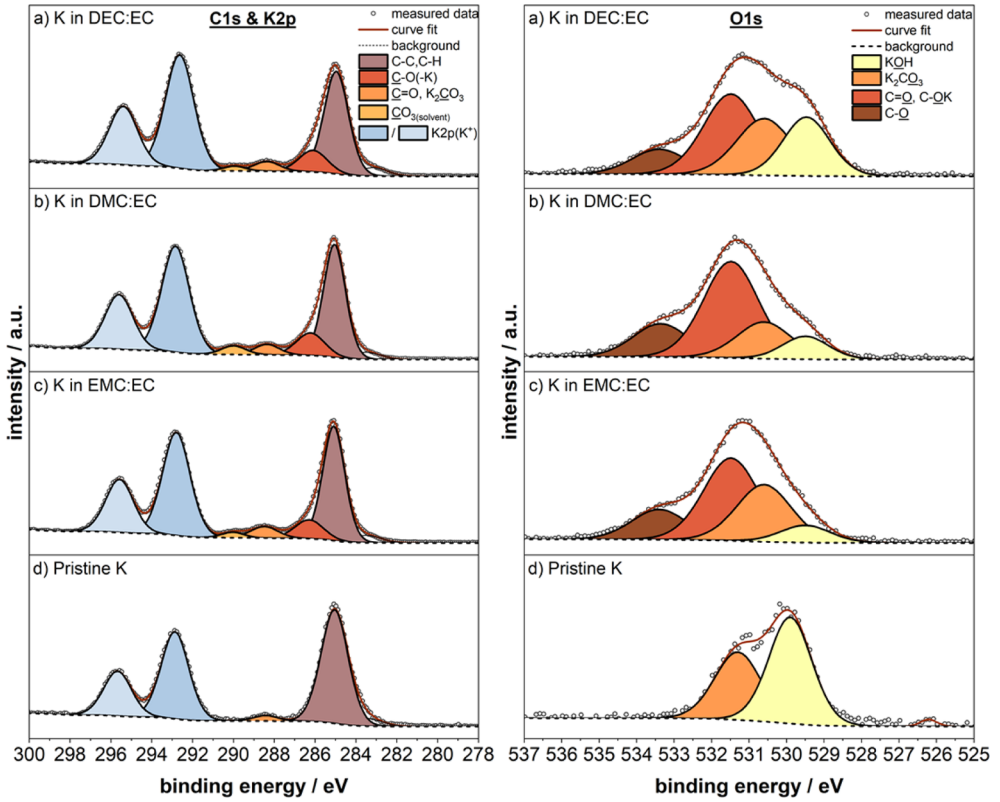

Figure 14. C 1s and K 2p and O 1s spectra of the potassium surfaces after a storage time of 2 min in different solvent mixtures: DEC/EC (a) DMC/EC (b), and EMC/EC (c). For a better comparison of surface formation products, the spectra for pristine potassium, prepared as mentioned in the experimental part, without addition of solvent (d) are shown. The BE scale is calibrated versus the hydrocarbon peak at 285 eV.

https://doi.org/10.1021/acsami.4c17461
ACS Appl. Mater. Interfaces XXXX, XXX, XXX−XXX

Table 3. XPS Measurements on Stored Potassium in Various Solvent Compositions for 2 min with the Corresponding Peak Positions and Atom.-%

Storage time: 2 min	samples binding energy/eV (atomic concentration/atom-%)								
K in	C 1s C−C, C−H	C 1s−C−O−, −C−OK	C 1s-C═O−K_2CO_3	C 1s−(CO_3)−	K 2p	O 1s KOH	O 1s K_2CO_3	O 1sC═O, C−OK	O 1s C−O
EMC/EC	285 (43.5)	286.3 (9.2)	288.5 (5.4)	290.0 (2.1)	292.8 (16.0)	529.5 (2.0)	530.6 (7.4)	531.5 (10.7)	533.4 (3.9)
DMC/EC	285 (41.0)	286.2 (10.5)	288.4 (4.3)	290.0 (3.5)	292.9 (16.0)	529.5 (2.6)	530.6 (4.8)	531.5 (12.9)	533.4 (4.4)
DEC/EC	285 (42.0)	286.1 (10.3)	288.4 (4.2)	290.0 (1.8)	292.7 (17.8)	529.5 (5.6)	530.6 (6.4)	531.5 (9.1)	533.4 (2.8)

charge analysis, and (4) quantification of the surface layer composition.

3.2. Sputter Depth Profiling Analysis. The C 1s XPS spectra from the pristine K metal in Figure 13a exhibit an adventitious carbon peak at a BE of 285.0 eV and a minor peak at 288.4 eV (C═O, K_2CO_3) and a characteristic K 2p doublet at 292.7 eV (K $2p_{3/2}$), suggesting potassium salts at the surface.[45] The O 1s spectra of the pristine K metal in Figure 13a is dominated by the KOH peak at 529.8 eV. A second peak at 531.1 eV indicates carbonate/carbonyl species.[45] A visible change of cut potassium metal occurs rapidly from shiny to matte within minutes, even inside a glovebox, indicating the formation of an initial surface layer.

The highly reactive potassium metal reacts with glovebox contaminations even with at H_2O and O_2 concentration of <0.1 ppm or inside the ultrahigh vacuum analysis chamber of the XP spectrometer. In order to obtain a photoemission spectrum of the bare potassium metal surface, sputter depth profiling was performed using monatomic Ar^+-ion sputtering at 1000 eV (with etch phases: 4 × 40 s, 7 × 80 s, 7 × 160 s, 3 × 320 s) on the pristine K metal sample (cut and directly transferred into the vacuum system; no solvent exposure). Before Ar^+-ion sputtering, the outer layer of the initial K-metal surface is dominated by K_2CO_3 and KOH (Figure 13a), thus highlighting the formation of comparatively thick surface layers with minimal contaminants in the glovebox atmosphere. After sputtering, the content of K_2CO_3 as well as KOH is completely reduced and the K 2p signal of metallic potassium becomes the main component in the spectrum (Figure 13b). After a total sputter time of 2765 s, new sets of peaks appear in the K 2p region, while the carbon and oxygen components have been fully removed (see Figure 13b). The K 2p peak of metallic potassium is shifted to 291.9 eV and has a reduced full width at half-maximum (fwhm) of 0.70 eV compared to the signals from K^+ with a fwhm of 1.67 eV. In addition, the appearance of the plasmon peaks can be observed at BE above the K $2p_{1/2}$ signal up until BEs of 302 eV. These results clearly indicate a metallic potassium surface.[9,46] The C 1s, K 2p, and O 1s spectrum for sputtered K differs from the pristine K metal, which is commonly used in half cell test. This initial layer is crucial as it is likely to vary depending on the contaminants present in the glovebox, such as residues from previously used fluorine or sulfur containing electrolytes. These variations in the initial SEI, which has already produced various degradation products with the solvents alone (see the GC−MS section), may contribute to inconsistent and incomparable data. A representative potassium electrode preparation method in state-of-the-art literature is to prepare foils by rolling the soft metallic pieces in a plastic bag. XPS measurements showed the formation of an initial surface layer containing adventitious carbon, KOH, and K_2CO_3 with a higher KOH content compared to K_2CO_3, when using a plastic bag. In the literature, alternative preparation methods are also suggested through various pretreatments to reduce the amount of surface contaminants.

3.3. Solvent-Exposed Potassium Metal Surfaces. *3.3.1. C 1s-K 2p Spectra.* The K 2p spectra of the pristine K metal (Figure 14d), as well as the 2 min solvent-exposed samples (Figure 14a−c and Table 3), show the characteristic doublet at 292.7 eV (K $2p_{3/2}$), in accordance with previously reported values by our group.[6] This peak summarizes all potassium salts (K_2CO_3, KOH, and K-OR), thus suggesting that there is no metallic potassium visible in the XPS spectra. In addition, characteristic inorganic potassium components (K_2CO_3, $K_2C_2O_4$, CH_3CO_2K, and $KHCO_3$) were measured to facilitate the assignment process and to expand the existing XPS database of SEI characteristic compounds for potassium-related cells.[45] The core level spectra can be found in the Supporting Information, Figure S29. The BE shifts of the O 1s and C 1s-K 2p regions are given in Table S6. The samples exposed to the solvent mixtures showed four C 1s peaks, at binding energies of 285.0 eV (C−C, C−H), 286.3 eV (C−O, R−OK, R/alkyl), 288.4 eV (C═O, K_2CO_3), and 289.9 eV (CO_3). The peak at lower BE at 286.3 eV could be attributed to carbon in −COK, indicating an alkoxide species like CH_3OK or CH_3CH_2OK, while the corresponding O 1s peak was observed at 531.4 eV.

Based on previous literature assignments and the reference measurements, the peak at 286.3 eV could be attributed to a mixture of two species, namely, C−O (expected slightly higher at 286.5 eV) and the alkoxide species which shifts the peak to lower BE.[45,47] Similarly, the peak at 288.4 eV could be a superposition of a carbonyl (C═O; expected at 287.9 eV) and carbonate (K_2CO_3, expected at 288.6 eV) species.

The BE of 289.9 eV is ascribed to the carbonate peak. At higher binding energies, organic carbonates are found at the sample surface, including (trapped) solvent residues or degradation products that derive from the compounds described in the GC−MS section above. These degradation products are most likely the salts of the corresponding organic carbonates formed once they lose their end groups. In comparison to the pristine K metal, only the C═O/K_2CO_3 peak is visible (see Figure 14d). This suggests that the distinction between CO_3-species attributed to K_2CO_3 and organic carbonates is possible.

3.3.2. O 1s Spectra. The O 1s spectra of the solvent exposed K metal samples in Figure 14a−c comprise four components. In addition to the KOH peak at 529.8 eV and the carbonate/carbonyl species at 531.1 eV, the solvent exposed samples

https://doi.org/10.1021/acsami.4c17461
ACS Appl. Mater. Interfaces XXXX, XXX, XXX−XXX

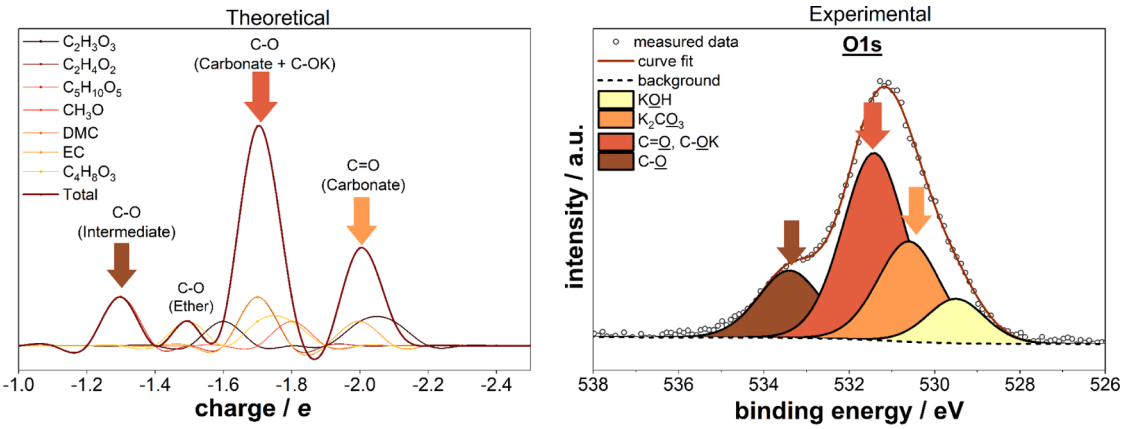

Figure 15. Comparison of charge analysis results for carbon and measured XPS O 1s spectra for potassium stored in the DMC/EC mixture. The results are plotted in units of electron charge/e ($1.602176634 \times 10^{-19}$ C), which directly correlates to units of eV in the photoemission spectra.

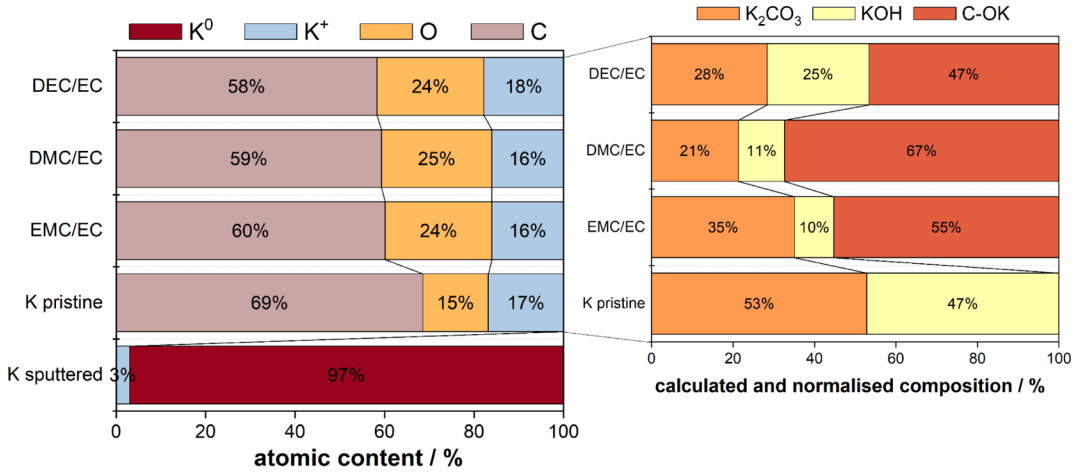

Figure 16. Bar plots of the calculated atomic concentration in percent of (a) main surface elements, i.e., carbon, oxygen, and potassium and (b) main surface specie, carbonates, hydroxide, and alkoxide species on the potassium metal, which were normalized to 1 and calculated on the basis of the detailed bar plot (Figure S31).

(Figure 14a–c) show additionally alkoxide- and alcoholate (C–O) species at 531.5 and 533.4 eV.[45]

3.3.3. Charge Analysis. Andersson et al. recently demonstrated that a Bader charge analysis is effective even without performing X-ray absorption near edge structure calculations.[48] Leveraging the theoretical results in this work, we attempted to correlate the BE differences of fitted peaks in the photoemission O 1s and C 1s spectra based on the calculated atomic charges. This method of charge analysis produces a collection of spectra for the calculated decomposition products identified in previous sections. The results are plotted in units of electron charge/e ($1.602176634 \times 10^{-19}$ C), which directly correlates to units of eV in the photoemission spectra.

3.3.4. O 1s Spectra. The O 1s XPS spectra from the storage experiment of potassium in DMC/EC shows four main peaks with (C–O) at 533.4 eV and C═O/C–O–K at 531.5 eV as well as carbonates (K_2CO_3) and hydroxides (KOH) at 530.6 and 529.5 eV. The experimental XPS spectra are in good agreement with the predicted hierarchy of the oxygen charges, as shown in Figure 15. While the theoretical intensities are arbitrary and do not hold any physical meaning, the relative shift of the charge of the respective oxygen atom can be correlated with the shift in the XPS spectra (see Figure 14b). Here the main peak also originates from the C–O (alkoxid) species at −1.7e, followed by the C═O (carbonate)-bonded oxygen with a charge of −2e and the smallest charge on the C–O (intermediate) at −1.3e. The peak position of the suggested intermediate would be expected to overlap with the ether peak; however, due to the relative instability of the intermediate, it is unlikely that it can be detected by XPS measurement. It is further important to note that the C–O (ether) species at −1.5e is likely also contained within the same experimental peak as the intermediate.

3.3.5. C 1s Spectra. While the predicted charge of the oxygen atoms is in relatively good agreement with the experimental data, the calculated charges for the carbon atoms do not match as well (Figure 14b); in particular, the predicted +4e charge of the carbonate carbon is a very poor fit. This is likely due to the used charge analysis method overestimating the charge on the carbonate carbon. The theoretical charge distribution for the C 1s region predicts the largest charge on the carbonate oxygen of −2e, followed by C–O–K bonded oxygens with a charge of −1.7e and the smallest charge on the ether oxygen of −1.5e. The charge values for each fragment are depicted in the figures in the Supporting Information (Figure S30).

3.3.6. Surface Layer Contents. Based on the fitted spectra, a quantification of the surface species was performed using

https://doi.org/10.1021/acsami.4c17461
ACS Appl. Mater. Interfaces XXXX, XXX, XXX–XXX

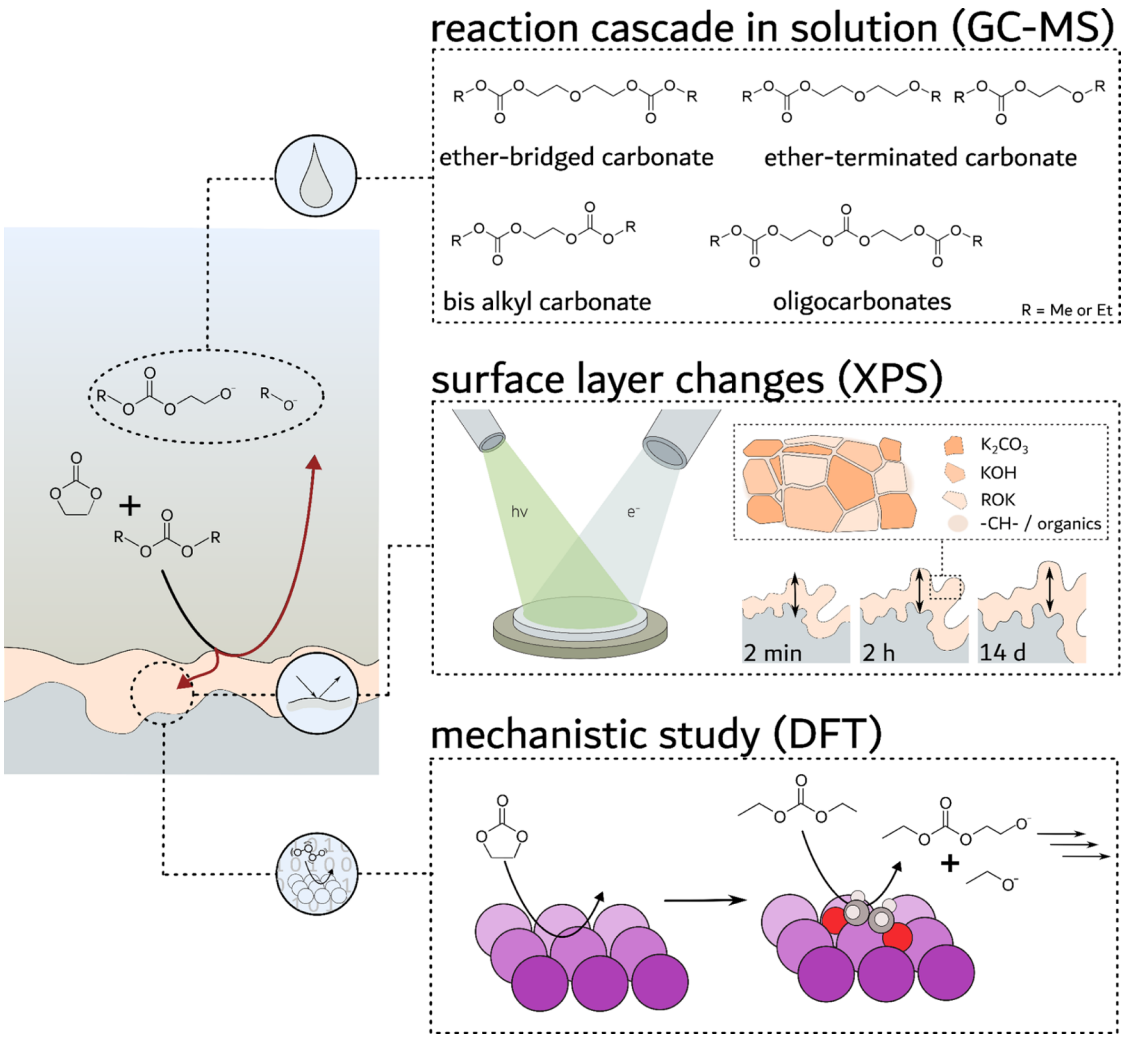

Figure 17. Schematic illustration of the methodology and research results, which are discussed in the following section in detail.

relative sensitivity factors. Figure 16a shows the relative atomic concentration of the three dominant elements, carbon, oxygen, and potassium. The atomic concentrations of C (≈59 ± 1 at. %), O (≈24 ± 1 at. %), and K (≈17 ± 1 at. %) are about the same for all three solvent mixtures within the accuracy of the quantification (±5 at. %). Surprisingly, it was found that the pristine K-foil displayed similar potassium contents than the solvent-exposed samples, but higher amounts of carbon (69 at %) and notably lower amounts of oxygen (15 at %).

The relative contents of the three dominant chemical compounds, namely, KOH, K_2CO_3, and R−OK (alcoholates), are further specified in Figure 16b. A more detailed bar plot with all listed values can be found in the Supporting Information, Figure S31.

For the pristine K sample, these are only KOH and K_2CO_3 in about similar amounts. In contrast, the KOH content decreases considerably in contact with carbonate solvents, in favor of alkoxide species. As discussed above, the formation of ethylene glycolate from EC is one of the central components in the further degradation cascade (Figure 11) of the soluble decomposition products in the first section. In EC/DMC mixtures, the R−OK formation appears to be particularly pronounced, in agreement with earlier GC−MS studies showing rapid formation of DMDD (compared to DEDD).[11] Notably, the DEC/EC sample contains approximately twice the amount of KOH in comparison to the K-metal samples exposed to the DMC/EC and EMC/EC samples. Moreover, EMC/EC contains the highest proportion of K_2CO_3, amounting to 35 at. %. Both finding for DEC and EMC-based mixtures might hint toward different degrees of surface interactions and reactivities in the respective linear carbonates.

3.4. Evaluation of the Reaction Products Formed upon Mixing Solvents with Individual Potassium Salts.

In order to ascertain the impact of the formed interphase of potassium on the solvent, a series of experiments was conducted, in which several potassium salts (KOH, K_2CO_3, KO_2, and KOEt) were dissolved in the solvent DEC/EC and analyzed using GCMS after a reaction time of 1 week. The decomposition products detected in the solvent, along with the corresponding reference measurements, are presented in Figures S32−S34 (Supporting Information), and the assigned compounds are listed in Table S7 (Supporting Information).

The reference measurement (pure DEC/EC) did not indicate the presence of any degradation product in the solvent. As previously stated, the addition of potassium metal results in the formation of DEDD as the primary degradation product.[11] It is shown that the addition of KOH as well as K_2CO_2 had almost no impact and did not result in the formation of significant degradation products. However, when potassium oxide (KO_2) was added, a pronounced formation of

https://doi.org/10.1021/acsami.4c17461
ACS Appl. Mater. Interfaces XXXX, XXX, XXX−XXX

DEDD is observed. Conversely, the addition of KOEt to DEC/EC results in the pronounced formation of various products, including ethanol, DEDD (**13**), and DECE (**15**), along with unidentified degradation products.[28]

4. DISCUSSION

In this work, we explored how different carbonate-based solvent combinations react in contact with potassium metal. In our comprehensive analysis, the soluble degradation products that accumulated in the bulk solvent phase were investigated in great detail by GCMS. Insoluble deposits from solvent decomposition on the potassium surface were analyzed by XPS. For a deeper mechanistic understanding of the degradation processes, the results were linked to ab initio DFT calculations. The methodology and research results are presented in Figure 17.

When mixtures of linear carbonates (DMC, DEC, and EMC) and cyclic carbonates (EC) react at the potassium metal surface (in the absence of electrolyte salt), ethylene bis(alkyl carbonates) (**5**, **6**, and **13**) are formed. Laruelle and co-workers described these compounds previously as "telltales" to the electrolyte health (in Li-systems).[49,50] As soluble species, they accumulate in the liquid electrolyte phase. As shown herein, and in previous works, their concentration increases significantly in the presence of potassium, as compared to lithium.[11,45] In this study, we presented the rich chemistry that evolves around the initial bis(alkyl carbonates) to a variety of oligomeric species, comprising alkyl carbonate-, ether-, or mixed-terminated end groups. Their concentration in the solvent mixtures is comparatively small, even after 14 days of exposure to K-metal. Hence, some species were observed only after further concentration of the analyte. The same compounds were found in electrolyte mixtures (including conducting salt) that were exposed to lithium metal, as previously reported by Gachot et al.[28,43]

Following these earlier works, radical intermediates are often suggested to initiate the formation of the ethylene bis(alkyl carbonates).[28,43] It is proposed that these species are formed through electron transfer reactions from the alkali metal to the linear carbonate or EC.[28,49,50] However, these reactions are performed usually using conducting salts (e.g., $LiPF_6$) as well as cell potential, which are both not present here. As a byproduct of the degradation of the linear carbonate, alkoxides are formed, which are involved in a variety of nucleophilic reactions with the soluble degradation compounds (Table 1). In our ab initio DFT calculation, the most favorable reaction pathway was the formation of a surface adsorbed glycolate intermediate species from EC. In comparison, the fragmentation of the linear carbonates turned out to be unlikely. This is in agreement with our previous study, where notable contents of degraded solvent species were observed only when both EC and a linear carbonate was present. The glycolate intermediate plays a function similar to that of the methanolate (MeO^-) in reaction mechanisms proposed in earlier works, through nucleophilic attacks at the sp^2-hybridized carbon center of the carbonate functional group (Figure 9). In the process, one equivalent of RO^- is formed that can participate in subsequent reactions to form the variety of compounds, such as DECE (**15**) and EEEC (**12**), from the original ethylene bis(alkyl carbonate). It should be noted that charged species such as RO^- cannot be analyzed directly by GCMS. Previous studies used scavengers to determine the alkoxide amounts.[50] However, the buildup of the alkoxide concentration in correlation to the ethylene bis(alkyl carbonate) concentration is a relevant topic for future investigations.

Furthermore, the surface analysis of potassium metal clearly demonstrated a significant contribution of alkoxides at the surface, while pristine potassium samples comprised solely of potassium carbonate (from the reaction of EC to K_2CO_3 and C_2H_4) and potassium hydroxide from residual moisture.[8] The peak position of the suggested intermediate would be expected to overlap with the ether peak, however due to the relative instability of the intermediate it is unlikely that it can be detected by XPS measurement. Our analysis further revealed that a thick surface layer forms rapidly even on freshly prepared potassium surfaces with minimal exposure times to the glovebox atmosphere. The potassium signal in photoemission spectra of potassium metal was found to originate solely from potassium salts, suggesting that the surface layer is thicker than the probing depth of the in-house XPS (<10 nm).[51,52] Only after longer (monatomic) Ar^+ etching did the characteristic metallic features of potassium appear. The K 2p signal shifted to lower binding energies by 0.8 eV, and several plasmon peaks appeared in the same range. Even under the ultrahigh vacuum conditions in the XPS analysis chamber, a surface layer regrew on the metallic surface after sputtering during a 1 h storage. This result highlights the reactivity of the alkali metal and may give rise to comparability issues between different (half cell) studies, as the potassium surface composition (prior to cell assembly) can be very dependent on the glovebox atmosphere. Interestingly, KOH and K_2CO_3 had only a minor impact on the ethylene bis(alkyl carbonate) formation, while the presence of potassium oxides and alkoxides was found to promote the formation of the soluble degradation products rapidly.

The GCMS analysis was a qualitative, nonquantitative approach; therefore, only limited conclusions could be drawn regarding the amount of degradation products or their potential increase over time. Nevertheless, using the same procedure for each analysis allowed for comparative evaluation, e.g., the difference between DMC, DEC, and EMC as well as the time-dependent formation within 14 days. XPS experiments over longer exposure times showed an ongoing degradation process that led to an increased layer thickness. After 14 days, the layer became too thick for meaningful analysis due to strong charging effects.

Overall, a variety of carbonate- and/or ether-terminated degradation products are formed through mediation of the potassium metal surface. Their formation is independent of the presence of electrolyte salt, although the presence of anions, such as PF_6^- leads to further branching of the reaction pathways and addition of decomposition compounds. Because of their comparatively high concentrations in contact with metallic potassium, they may interfere with the cell reactions in KIBs, owing to crosstalk phenomena. As shown recently, in some instances, their presence can be even noted as an additional features in the voltage profiles of the Prussian white positive electrodes.[53] Similarly, lower concentrations of degradation compounds in EC/DEC mixtures lead to longer cycle life for graphite/K-metal half cells in another previous study.[11] However, these solvents represent only a small selection of frequently used solvents for battery electrolytes. In order to derive general electrolyte design principles other commonly used solvents, e.g., propylene carbonate,[54,55] and their interactions with other solvent components need to be investigated in more detailed in future studies.

https://doi.org/10.1021/acsami.4c17461
ACS Appl. Mater. Interfaces XXXX, XXX, XXX−XXX

5. CONCLUSIONS

The results described herein show a combined theoretical and experimental approach to understanding the initial degradation steps that lead to the formation of the initial interphase on potassium metal in contact with various carbonate-based solvent combinations. By correlating the adsorption behavior of decomposition products with their detectability within the GCMS and XPS setup with DFT calculations, we successfully linked the different scales of the different techniques, ranging from the Angstrom/nm and fs/ps scale of DFT to the minute-to-day scale of experiments in the laboratory. Measurements on the pristine potassium metal surface showed that the surface layer is influenced early on due to adsorption of residual moisture and contaminants both inside the glovebox and under ultrahigh vacuum (UHV) conditions of the XPS chamber. The addition of different solvent mixtures changed the surface composition on the potassium metal by forming a potassium alkoxide. Similar, solvent degradation was observed resulting in di- and tricarbonate-functionalized oligomers, ether-bridged carbonates, and ether-like products. We provide retention time indexes of such compounds in order to be able to detect and identify substances regardless of the GCMS setup. By combining the insights gained from experimental measurements and theoretical simulations, we could not only identify changes in the decomposition process of the solvents but also propose a possible mechanism by which these changes occur. Specifically, we suggested that EC decomposition produces ethylene glycolate, which connects the carbonate groups in DMC and DEC, underscoring the crucial role of EC decomposition in these reactions. We propose that the reaction proceeds forming a $C_4H_7O_4$ intermediate via methoxycarbonylation, producing alkoxide as a byproduct. The abundance of potassium alkoxide on the potassium metal within the XPS measurements supports these findings.

This study provides an initial step to understand solvent decomposition and provides detailed mechanistic insights that may be applicable beyond the scope of this solvent combination. It can serve as a reference for more complex systems involving conducting salts.

However, further research is required to determine how the reaction proceeds to form longer (poly)ethylene glycol connectors as well as if these oligomers form without EC, thereby confirming the role of the EC decomposition products.

■ ASSOCIATED CONTENT

Data Availability Statement

Raw data: raw data of the GC and XPS measurements as well as the calculations are available at Zenodo.org (10.5281/zenodo.14409083).

Supporting Information

The Supporting Information is available free of charge at https://pubs.acs.org/doi/10.1021/acsami.4c17461.

Additional experimental details, materials, and methods, including XPS experimental details, GCMS data, NMR data of decomposition products, list of all chemicals and decomposition products, chromatograms of DMC, EMC and DEC, mass spectra at defined retention times as well as mass fragmentation data of decomposition products, time-dependent electrolyte decomposition, calculated DOS plots and Bader charges for the investigated fragments, formation and adsorption energies of the calculated fragments, XPS data on potassium and reference samples, and GCMS data of EC/DEC mixtures including selected potassium salts (PDF)

■ AUTHOR INFORMATION

Corresponding Author

Andreas Hofmann − *Institute for Applied Materials, Karlsruhe Institute of Technology, 76344 Eggenstein-Leopoldshafen, Germany;* orcid.org/0000-0002-9102-7641; Email: andreas.hofmann2@kit.edu

Authors

Leonie Wildersinn − *Institute for Applied Materials, Karlsruhe Institute of Technology, 76344 Eggenstein-Leopoldshafen, Germany*

Daniel Stottmeister − *Helmholtz Institute Ulm Electrochemical Energy Storage, Institute of Theoretical Chemistry Ulm University, 89069 Ulm, Germany*

Fabian Jeschull − *Institute for Applied Materials, Karlsruhe Institute of Technology, 76344 Eggenstein-Leopoldshafen, Germany;* orcid.org/0000-0002-5927-1978

Axel Groß − *Helmholtz Institute Ulm Electrochemical Energy Storage, Institute of Theoretical Chemistry Ulm University, 89069 Ulm, Germany;* orcid.org/0000-0003-4037-7331

Complete contact information is available at: https://pubs.acs.org/10.1021/acsami.4c17461

Author Contributions

A.H.: Conceptualization (lead), investigation (equal), formal analysis (equal), resources (equal), visualization, writing—original draft preparation (equal), writing—review and editing (equal), and supervision (equal). **D.S.**: Investigation (equal), formal analysis (equal), writing—original draft preparation (equal), and writing—review and editing (equal). **F.J.**: Conceptualization (support), resources (equal), supervision (equal), writing—original draft preparation (equal), and writing—review and editing (equal). **A.G.**: Resources (equal), supervision (equal), writing—review and editing (equal). **L.W.**: Investigation (equal), formal analysis (equal), visualization, writing—original draft preparation (equal), and writing—review and editing (equal).

Notes

The authors declare no competing financial interest.

■ ACKNOWLEDGMENTS

This work contributes to the research performed at CELEST (Center for Electrochemical Energy Storage Ulm-Karlsruhe) and was funded by the German Research Foundation (DFG) under Project ID 390874152 (POLiS Cluster of Excellence).

■ REFERENCES

(1) Hosaka, T.; Kubota, K.; Hameed, A. S.; Komaba, S. Research Development on K-Ion Batteries. *Chem. Rev.* **2020**, *120*, 6358−6466.

(2) Hosaka, T.; Matsuyama, T.; Tatara, R.; Gossage, Z. T.; Komaba, S. Impact of electrolyte decomposition products on the electrochemical performance of 4 V class K-ion batteries. *Chem. Sci.* **2023**, *14*, 8860−8868.

(3) Xu, Y.; Titirici, M.; Chen, J.; Cora, F.; Cullen, P. L.; Edge, J. S.; Fan, K.; Fan, L.; Feng, J.; Hosaka, T.; et al. roadmap for potassium-ion batteries. *J. Phys. Energy* **2023**, *5*, 021502−021574.

(4) Larcher, D.; Tarascon, J.-M. Towards greener and more sustainable batteries for electrical energy storage. *Nat. Chem.* **2015**, *7*, 19−29.

(5) Pham, T. A.; Kweon, K. E.; Samanta, A.; Lordi, V.; Pask, J. E. Solvation and Dynamics of Sodium and Potassium in Ethylene Carbonate from ab Initio Molecular Dynamics Simulations. *J. Phys. Chem. C* **2017**, *121*, 21913−21920.
(6) Allgayer, F.; Maibach, J.; Jeschull, F. Comparing the Solid Electrolyte Interphases on Graphite Electrodes in K and Li Half Cells. *ACS Appl. Energy Mater.* **2022**, *5*, 1136−1148.
(7) Madec, L.; Gabaudan, V.; Gachot, G.; Stievano, L.; Monconduit, L.; Martinez, H. Paving the Way for K-Ion Batteries: Role of Electrolyte Reactivity through the Example of Sb-Based Electrodes. *ACS Appl. Mater. Interfaces* **2018**, *10*, 34116−34122.
(8) Caracciolo, L.; Madec, L.; Gachot, G.; Martinez, H. Impact of the Salt Anion on K Metal Reactivity in EC/DEC Studied Using GC and XPS Analysis. *ACS Appl. Mater. Interfaces* **2021**, *13*, 57505−57513.
(9) Dhir, S.; Jagger, B.; Maguire, A.; Pasta, M. Fundamental investigations on the ionic transport and thermodynamic properties of non-aqueous potassium-ion electrolytes. *Nat. Commun.* **2023**, *14*, 3833.
(10) Larhrib, B.; Madec, L. Toward Highly Reliable Potassium-Ion Half and Full Coin Cells. *Batteries Supercaps* **2023**, *6*, No. e202300061.
(11) Hofmann, A.; Müller, F.; Schöner, S.; Jeschull, F. Revealing the Formation of Dialkyl Dioxahexane Dioate Products from Ethylene Carbonate based Electrolytes on Lithium and Potassium Surfaces. *Batteries Supercaps* **2023**, *6*, No. e202300325.
(12) Hosaka, T.; Fukabori, T.; Matsuyama, T.; Tatara, R.; Kubota, K.; Komaba, S. 1,3,2-Dioxathiolane 2,2-Dioxide as an Electrolyte Additive for K-Metal Cells. *ACS Energy Lett.* **2021**, *6*, 3643−3649.
(13) Gu, M.; Fu, H.; Rao, A. M.; Zhou, J.; Lin, Y.; Wen, S.; Fan, L.; Lu, B. In Situ Construction of Uniform and Elastic Solid−Electrolyte Interphase for High-Performance Potassium Batteries. *Adv. Funct. Mater.* **2024**, *34*, 2407867.
(14) Bie, X.; Kubota, K.; Hosaka, T.; Chihara, K.; Komaba, S. A novel K-ion battery: hexacyanoferrate(II)/graphite cell. *J. Mater. Chem. A* **2017**, *5*, 4325−4330.
(15) Deng, L.; Zhang, Y.; Wang, R.; Feng, M.; Niu, X.; Tan, L.; Zhu, Y. Influence of KPF_6 and KFSI on the Performance of Anode Materials for Potassium-Ion Batteries: A Case Study of MoS_2. *ACS Appl. Mater. Interfaces* **2019**, *11*, 22449−22456.
(16) Khudyshkina, A. D.; Morozova, P. A.; Butzelaar, A. J.; Hoffmann, M.; Wilhelm, M.; Theato, P.; Fedotov, S. S.; Jeschull, F. Poly(ethylene oxide)-Based Electrolytes for Solid-State Potassium Metal Batteries with a Prussian Blue Positive Electrode. *ACS Appl. Polym. Mater.* **2022**, *4*, 2734−2746.
(17) Wang, H.; Yu, D.; Wang, X.; Niu, Z.; Chen, M.; Cheng, L.; Zhou, W.; Guo, L. Electrolyte Chemistry Enables Simultaneous Stabilization of Potassium Metal and Alloying Anode for Potassium-Ion Batteries. *Angew. Chem., Int. Ed.* **2019**, *58*, 16451−16455.
(18) Fan, L.; Xie, H.; Hu, Y.; Caixiang, Z.; Rao, A. M.; Zhou, J.; Lu, B. A tailored electrolyte for safe and durable potassium ion batteries. *Energy Environ. Sci.* **2023**, *16*, 305−315.
(19) Wang, H.; Zhai, D.; Kang, F. Solid electrolyte interphase (SEI) in potassium ion batteries. *Energy Environ. Sci.* **2020**, *13*, 4583−4608.
(20) Stottmeister, D.; Groß, A. Toward the Formation of the Solid Electrolyte Interphase on Alkaline Metal Anodes: Ab Initio Simulations. *Batteries Supercaps* **2023**, *6*, No. e202300156.
(21) Euchner, H.; Groß, A. Atomistic modeling of Li- and post-Li-ion batteries. *Phys. Rev. Mater.* **2022**, *6*, 040302−040328.
(22) Kresse, G.; Furthmüller, J. Efficient iterative schemes for *ab initio* total-energy calculations using a plane-wave basis set. *Phys. Rev. B* **1996**, *54*, 11169−11186.
(23) Hammer, B.; Hansen, L. B.; Nørskov, J. K. Improved adsorption energetics within density-functional theory using revised Perdew-Burke-Ernzerhof functionals. *Phys. Rev. B* **1999**, *59*, 7413−7421.
(24) Ehrlich, S.; Moellmann, J.; Reckien, W.; Bredow, T.; Grimme, S. System-Dependent Dispersion Coefficients for the DFT-D3 Treatment of Adsorption Processes on Ionic Surfaces. *ChemPhysChem* **2011**, *12*, 3414−3420.
(25) Mahlberg, D.; Sakong, S.; Forster-Tonigold, K.; Groß, A. Improved DFT Adsorption Energies with Semiempirical Dispersion Corrections. *J. Chem. Theory Comput.* **2019**, *15*, 3250−3259.
(26) Sotoudeh, M.; Baumgart, S.; Dillenz, M.; Döhn, J.; Forster-Tonigold, K.; Helmbrecht, K.; Stottmeister, D.; Groß, A. Ion Mobility in Crystalline Battery Materials. *Adv. Energy Mater.* **2024**, *14*, 2302550.
(27) Tang, W.; Sanville, E.; Henkelman, G. A grid-based Bader analysis algorithm without lattice bias. *J. Condens. Matter Phys.* **2009**, *21*, 084204−084210.
(28) Gachot, G.; Grugeon, S.; Armand, M.; Pilard, S.; Guenot, P.; Tarascon, J.-M.; Laruelle, S. Deciphering the multi-step degradation mechanisms of carbonate-based electrolyte in Li batteries. *J. Power Sources* **2008**, *178*, 409−421.
(29) Mönnighoff, X.; Murmann, P.; Weber, W.; Winter, M.; Nowak, S. Post-Mortem Investigations of Fluorinated Flame Retardants for Lithium Ion Battery Electrolytes by Gas Chromatography with Chemical Ionization. *Electrochim. Acta* **2017**, *246*, 1042−1051.
(30) Sasaki, T.; Abe, T.; Iriyama, Y.; Inaba, M.; Ogumi, Z. Formation mechanism of alkyl dicarbonates in Li-ion cells. *J. Power Sources* **2005**, *150*, 208−215.
(31) Sasaki, T.; Jeong, S.-K.; Abe, T.; Iriyama, Y.; Inaba, M.; Ogumi, Z. Effect of an Alkyl Dicarbonate on Li-Ion Cell Performance. *J. Electrochem. Soc.* **2005**, *152*, A1963−A1968.
(32) Schultz, C.; Kraft, V.; Pyschik, M.; Weber, S.; Schappacher, F.; Winter, M.; Nowak, S. Separation and Quantification of Organic Electrolyte Components in Lithium-Ion Batteries via a Developed HPLC Method. *J. Electrochem. Soc.* **2015**, *162*, A629−A634.
(33) Takeda, S.; Morimura, W.; Liu, Y.-H.; Sakai, T.; Saito, Y. Identification and formation mechanism of individual degradation products in lithium-ion batteries studied by liquid chromatography/electrospray ionization mass spectrometry and atmospheric solid analysis probe mass spectrometry. *Rapid Commun. Mass Spectrom.* **2016**, *30*, 1754−1762.
(34) Grützke, M.; Weber, W.; Winter, M.; Nowak, S. Structure determination of organic aging products in lithium-ion battery electrolytes with gas chromatography chemical ionization mass spectrometry (GC-CI-MS). *RSC Adv.* **2016**, *6*, 57253−57260.
(35) von Holtum, B.; Kubot, M.; Peschel, C.; Rodehorst, U.; Winter, M.; Nowak, S.; Wiemers-Meyer, S. Accessing the Primary Solid−Electrolyte Interphase on Lithium Metal: A Method for Low-Concentration Compound Analysis. *ChemSusChem* **2023**, *16*, No. e202201912.
(36) Tundo, P.; Memoli, S.; Hérault, D.; Hill, K. Synthesis of methylethers by reaction of alcohols with dimethylcarbonate. *Green Chem.* **2004**, *6*, 609−612.
(37) Chan, J. M. W.; Zhang, X.; Brennan, M. K.; Sardon, H.; Engler, A. C.; Fox, C. H.; Frank, C. W.; Waymouth, R. M.; Hedrick, J. L. Organocatalytic Ring-Opening Polymerization of Trimethylene Carbonate To Yield a Biodegradable Polycarbonate. *J. Chem. Educ.* **2015**, *92*, 708−713.
(38) Zhuang, G. V.; Yang, H.; Ross, P. N.; Xu, K.; Jow, T. R. Lithium Methyl Carbonate as a Reaction Product of Metallic Lithium and Dimethyl Carbonate. *Electrochem. Solid-State Lett.* **2006**, *9*, A64−A68.
(39) Fiorani, G.; Perosa, A.; Selva, M. Dimethyl carbonate: a versatile reagent for a sustainable valorization of renewables. *Green Chem.* **2018**, *20*, 288−322.
(40) Tundo, P.; Musolino, M.; Aricò, F. The reactions of dimethyl carbonate and its derivatives. *Green Chem.* **2018**, *20*, 28−85.
(41) Saito, K.; Jehanno, C.; Meabe, L.; Olmedo-Martínez, J. L.; Mecerreyes, D.; Fukushima, K.; Sardon, H. From plastic waste to polymer electrolytes for batteries through chemical upcycling of polycarbonate. *J. Mater. Chem. A* **2020**, *8*, 13921−13926.
(42) Stottmeister, D.; Wildersinn, L.; Maibach, J.; Hofmann, A.; Jeschull, F.; Groß, A. Unraveling Propylene Oxide Formation in Alkali Metal Batteries. *ChemSusChem* **2024**, *17*, No. e202300995.

https://doi.org/10.1021/acsami.4c17461
ACS Appl. Mater. Interfaces XXXX, XXX, XXX−XXX

(43) Gachot, G.; Ribière, P.; Mathiron, D.; Grugeon, S.; Armand, M.; Leriche, J.-B.; Pilard, S.; Laruelle, S. Gas Chromatography/Mass Spectrometry As a Suitable Tool for the Li-Ion Battery Electrolyte Degradation Mechanisms Study. *Anal. Chem.* **2011**, *83*, 478−485.
(44) Gireaud, L.; Grugeon, S.; Pilard, S.; Guenot, P.; Tarascon, J.-M.; Laruelle, S. Mass Spectrometry Investigations on Electrolyte Degradation Products for the Development of Nanocomposite Electrodes in Lithium Ion Batteries. *Anal. Chem.* **2006**, *78*, 3688−3698.
(45) Caracciolo, L.; Madec, L.; Martinez, H. XPS Analysis of K-based Reference Compounds to Allow Reliable Studies of Solid Electrolyte Interphase in K-ion Batteries. *ACS Appl. Energy Mater.* **2021**, *4*, 11693−11699.
(46) Oswald, S.; Gorbunov, M. V.; Mikhailova, D. Electron spectroscopy investigations of potassium and potassium-intercalated graphite with battery background. *Appl. Suf. Sci.* **2024**, *655*, 159614−159623.
(47) Gu, M.; Rao, A. M.; Zhou, J.; Lu, B. In situ formed uniform and elastic SEI for high-performance batteries. *Energy Environ. Sci.* **2023**, *16*, 1166−1175.
(48) Andersson, E. K. W.; Wu, L.-T.; Bertoli, L.; Weng, Y.-C.; Friesen, D.; Elbouazzaoui, K.; Bloch, S.; Ovsyannikov, R.; Giangrisostomi, E.; Brandell, D.; et al. Initial SEI formation in LiBOB-, LiDFOB- and $LiBF_4$-containing PEO electrolytes. *J. Mater. Chem. A* **2024**, *12*, 9184−9199.
(49) Eshetu, G. G.; Grugeon, S.; Kim, H.; Jeong, S.; Wu, L.; Gachot, G.; Laruelle, S.; Armand, M.; Passerini, S. Comprehensive Insights into the Reactivity of Electrolytes Based on Sodium Ions. *ChemSusChem* **2016**, *9*, 462−471.
(50) Kim, H.; Grugeon, S.; Gachot, G.; Armand, M.; Sannier, L.; Laruelle, S. Ethylene bis-carbonates as telltales of SEI and electrolyte health, role of carbonate type and new additives. *Electrochim. Acta* **2014**, *136*, 157−165.
(51) *NIST Standard Reference Database 71*; NIST, 2010.
(52) Tanuma, S.; Powell, C. J.; Penn, D. R. Calculations of electron inelastic mean free paths. V. Data for 14 organic compounds over the 50−2000 eV range. *Surf. Interface Anal.* **1994**, *21*, 165−176.
(53) Panasenko, I.; Bäuerle, M.; Jeschull, F. How reference electrodes improve our understanding of degradation processes in half and full cell potassium-ion battery setups. *Electrochim. Acta* **2025**, *513*, 145551−145563.
(54) Hofmann, A.; Wang, Z.; Bautista, S. P.; Weil, M.; Müller, F.; Löwe, R.; Schneider, L.; Mohsin, I. U.; Hanemann, T. Dataset of propylene carbonate based liquid electrolyte mixtures for sodium-ion cells. *Data in Brief* **2022**, *40*, 107775−107792.
(55) Hofmann, A.; Wang, Z.; Bautista, S. P.; Weil, M.; Müller, F.; Löwe, R.; Schneider, L.; Mohsin, I. U.; Hanemann, T. Comprehensive characterization of propylene carbonate based liquid electrolyte mixtures for sodium-ion cells. *Electrochim. Acta* **2022**, *403*, 139670−139687.

https://doi.org/10.1021/acsami.4c17461
ACS Appl. Mater. Interfaces XXXX, XXX, XXX−XXX